

# A one-dimensional morphoelastic model for burn injuries: stability, numerical validation, and biological interpretation

Ginger Egberts · Fred Vermolen · Paul van Zuijlen

June 22, 2022

## Abstract

To deal with permanent deformations and residual stresses, we consider a morphoelastic model for the scar formation as the result of wound healing after a skin trauma. Next to the mechanical components such as strain and displacements, the model accounts for biological parameters such as the concentration of chemokines, the cellular densities of fibroblasts and myofibroblasts, and the density of collagen. We present separate stability constraints for the mechanical part of the one-dimensional morphoelastic model and stability constraints for the chemical part of the one-dimensional morphoelastic model. Stability results are developed for both the continuous and (semi-)discrete problems. For the mechanical part, we distinguish between elasticity and plasticity. We perform numerical validation to these constraints and provide a biological interpretation of the (in)stability. For the mechanical model, the results show that the components reach equilibria in a (non) monotonic way, depending on the value of the viscosity. Furthermore, the results show that the parameters of the chemical model need to meet the stability constraint to avoid unrealistic results.

## 1 Introduction

Burn wounds are a global problem and are the fifth most common cause of non-fatal childhood injuries. Figures show that the number of burn injuries was nearly 11 million worldwide in 2004, and about 180,000 people die from burns each year WHO (2018). Given that burns mainly occur at home and workplace and that particularly adult women and children are vulnerable to burns WHO (2018), targeting burn prevention specifically at these target groups results in lower numbers of incidents. Besides pain, itching, and loss of energy, mental factors and additional factors of wound healing play a role. Slow wound healing, infection, extreme pain, hypertrophic scars, and contractures remain as major challenges in burn management Wang (2018).

The wound healing process comprises four partially overlapping phases that normally act upon each other quickly. The first phase, haemostasis, begins almost immediately after injury and aims primarily at stopping bleeding and starting the second phase. Burn wound healing passes over haemostasis, by cause of burning and cauterization of blood vessels. Hence burn wound healing starts with the second phase of normal wound

healing, called the inflammatory response, which starts in just a few hours after injury to clean the wound and protects it against infections. The growth factors that play a major role stimulate angiogenesis and collagen metabolism Enoch and Leaper (2008) and activate cells, such as granulocytes (white blood cells) that play a major role in the continuation of the wound healing cascade.

During inflammation, the wound is cleaned and protected from bacterial infections, and the proliferative phase begins. These phases in wound healing are overlapping. The sub processes that take place during the proliferative phase are re-epithelialization, angiogenesis, fibroplasia and wound contraction. Sometimes, re-epithelialization never completes and skin grafting is necessary Young and McNaught (2011). The ultimate phase, remodeling and scar maturation, can take several years. This phase brings various processes and structures into balance. This results in a scar that, on average, has 50% strength of unwounded skin (within three months), and 80% on the long-term Enoch and Leaper (2008); Young and McNaught (2011).

Wound contraction is yet visible in small wounds: the edges of the wound pull in, the wound size reduces and the wounded area deforms. In adult patients, wounds can become 20-30% smaller over several weeks Olsen et al. (1995). Wound contraction involves a biomechanical interaction of fibroblasts, myofibroblasts, chemokines, and collagen. Depending on the wound dimensions (location on the body, size), and the extent of contraction, the result can cause reduced mobility. If the contraction result causes reduced mobility, then we commonly refer to a contracture. Contraction can lead to limited range-of-motion of joints, which can lead to immobility and is an important indication for scar revision.

Various studies report on mathematical models to predict the behavior of experimental and clinical wounds and to gain insight into which elements of the wound healing response might have a substantial influence on the contraction Tranquillo and Murray (1992); Olsen et al. (1995); Barocas and Tranquillo (1997); Dallon et al. (1999); McDougall et al. (2006); Koppenol (2017); Menon et al. (2017) to name a few. This study uses the morphoelastic model for burn wound contraction that has been developed by Koppenol in 2017. Morphoelasticity is based on the following principle Hall (2008): the total deformation is decomposed into a deformation as a result of growth or shrinkage and a deformation as a result of mechanical forces. In a mathematical context, one considers the following three coordinate systems:  $\mathbf{X}$ ,  $\mathbf{X}_e(t)$ , and  $\mathbf{x}(t)$ , which, respectively, represent the initial coordinate system, the equilibrium at time  $t$  that results due to growth or shrinkage, and the current coordinate system that results due to growth or shrinkage and mechanical deformation. Assuming sufficient regularity, the deformation gradient tensor is written by

$$\mathbf{F} = \frac{\partial \mathbf{x}}{\partial \mathbf{X}} = \frac{\partial \mathbf{x}}{\partial \mathbf{X}_e} \frac{\partial \mathbf{X}_e}{\partial \mathbf{X}} = \mathbf{A}\mathbf{Z}, \quad (1)$$

in which the tensor  $\mathbf{Z}$  represents the deformation gradient tensor due to growth or shrinkage, and  $\mathbf{A}$  represents the deformation gradient due to mechanical forces.

As an addition to the morphoelastic model developed by Koppenol, this study pro-

vides one-dimensional stability constraints as well as numerical validations of these constraints, and a biological interpretation of (in)stability.

The organization of this paper is as follows. Section 2 presents the mathematical model and Section 3 presents the stability analysis. Subsequently, Section 4 presents the numerical method that is used to approximate the solution and Section 5 presents the numerical validation of the stability constraints and a biological interpretation of (in)stability. Finally, Section 6 presents the conclusion and discussion.

## 2 The mathematical model

For the mathematical model we follow the assumption from Ramtani and et al (2002) and Ramtani (2004), in which we incorporate the dependence of the Young's modulus of skin on the density of collagen. The model considers the displacement of the dermal layer ( $u$ ), the displacement velocity of the dermal layer ( $v$ ) and the effective strain present in the dermal layer ( $\epsilon$ ). The effective strain is a local measure for the difference between the current configuration of the dermal layer and a hypothetical configuration of the dermal layer where the tissue is mechanically relaxed. Furthermore, we incorporate four constituents: the chemokines ( $c$ ), the fibroblasts ( $N$ ), the myofibroblasts ( $M$ ) and collagen ( $\rho$ ). Here we use collagen as a collective name for the molecules, fibrils and bundles of collagen.

We borrow the morphoelastic continuum hypothesis-based modeling framework from Koppenol (2017). The one-dimensional differential equations of this framework are

$$\frac{\partial z_i}{\partial t} + \frac{\partial(z_i v)}{\partial x} = -\frac{\partial J_i}{\partial x} + R_i, \quad (2)$$

$$\rho_t \left( \frac{\partial v}{\partial t} + 2v \frac{\partial v}{\partial x} \right) = \frac{\partial \sigma}{\partial x} + f, \quad (3)$$

$$\frac{\partial \epsilon}{\partial t} + v \frac{\partial \epsilon}{\partial x} + (\epsilon - 1) \frac{\partial v}{\partial x} = -G. \quad (4)$$

We bear in mind that due to the forces that are exerted by the cells, the domain deforms and hence the points within the domain of computation are subject to displacement. The local displacement rate is incorporated by *passive convection*, which is reflected by the second term in the left-hand sides in equations (2) to (4). Equation (2) represents the conservation of the concentrations of the chemokines, the (myo)fibroblast cell densities and collagen. Equation (3) is the conservation equation of linear momentum of the dermal layer. Equation (4) is the evolution equation that describes how the effective strain changes. The variable  $z_i$  in equation (2) represents the cell density / concentration of constituent  $i$ ,  $J_i$  represents the flux of constituent  $i$  per unit area and  $R_i$  represents the chemical kinetics associated with constituent  $i$ , given the constituents,  $i \in \{c, N, M, \rho\}$ . The constant  $\rho_t$  in equation (3) represents the total mass density of the dermal tissues.

In the rest of the text we replace  $z_i$  by  $i$ , so  $z_\rho$  becomes  $\rho$ , and so on. In the subsequent subsections we will show the constituent specific fluxes and chemical kinetics, the mechanical component, and plastic deformation (i.e., permanent contraction).

## 2.1 The chemokines

Chemokines are a family of small cytokines, or signaling proteins secreted by cells. During inflammation, chemokines are transported to the wounded area. They are necessary to effect, among other things, diffusion and proliferation of other cells. We assume that these chemokines diffuse through the dermal layer in a normal Fickian diffusion and that these chemokines spread randomly. Summarized in an equation, we obtain the following:

$$J_c = -D_c \frac{\partial c}{\partial x}. \quad (5)$$

Here  $D_c$  is the Fickian diffusion coefficient of the chemokines.

It is known that fibroblasts secrete chemokines. We assume that both fibroblasts and a proportion of myofibroblasts secrete and consume chemokines. Hence, the proliferation of the chemokines depends on the local distribution of the (myo)fibroblasts. Furthermore, a generic MMP removes chemokines from the dermal layer through proteolytic breakdown. The concentration of the generic MMP is proportional to the cell density of the (myo)fibroblast population, the concentration of collagen and the concentration of the chemokines. We assume that the chemokines also inhibit the secretion of the generic MMP. Hence summarized in an equation, we obtain the following reaction term:

$$R_c = k_c \left[ \frac{c}{a_c^{II} + c} \right] [N + \eta^I M] - \delta_c g(N, M, c, \rho) c, \quad (6)$$

where we follow Koppenol (2017) to assume that the concentration of the generic MMP is given by

$$g(N, M, c, \rho) = \frac{[N + \eta^{II} M] \rho}{1 + a_c^{III} c}. \quad (7)$$

In equation (6), the parameter  $k_c$  is the maximum net secretion rate of the chemokines,  $\eta^I$  is the ratio of myofibroblasts to fibroblasts in the maximum secretion rate of the chemokines,  $a_c^{II}$  is the concentration of the chemokines that causes the half-maximum net secretion rate of the chemokines, and  $\delta_c$  is the proteolytic breakdown rate parameter of the chemokines. In equation (7)  $\eta^{II}$  is the ratio of myofibroblasts to fibroblasts in the secretion rate of the MMPs and  $1/[1 + a_c^{III} c]$  represents the inhibition of the secretion of the generic MMP.

## 2.2 The (myo)fibroblasts

It is known that chemokines influence the chemotaxis of (myo)fibroblasts. Like for the chemokines, we assume that the cells diffuse randomly through the dermal layer according to linear Fickian diffusion. The random and directed movement (by chemotaxis) of the (myo)fibroblasts are therefore given by:

$$J_N = -D_F F \frac{\partial N}{\partial x} + \chi_F N \frac{\partial c}{\partial x}, \quad (8)$$

$$J_M = -D_F F \frac{\partial M}{\partial x} + \chi_F M \frac{\partial c}{\partial x}, \quad (9)$$

where  $F = N + M$ . The parameter  $D_F$  represents (myo)fibroblast random diffusion and  $\chi_F$  is the chemotactic parameter that depends on both the binding and unbinding rate of the chemokines with its receptor, and the concentration of this receptor on the cell surface of the (myo)fibroblasts.

The proliferation of the cells is incorporated into the model by using two similar logistic growth models. It is known that chemokines also influence the proliferation, differentiation and division of the cells. Hence, taking into account the chemokines, we obtain the following reaction equations:

$$R_N = r_F \left[ 1 + \frac{r_F^{\max} c}{a_c^I + c} \right] [1 - \kappa_F F] N^{1+q} - k_F c N - \delta_N N, \quad (10)$$

$$R_M = r_F \left[ \frac{[1 + r_F^{\max}] c}{a_c^I + c} \right] [1 - \kappa_F F] M^{1+q} + k_F c N - \delta_M M. \quad (11)$$

The three parts on the right hand side of equations (10) and (11) represent the proliferation, the differentiation from fibroblasts to myofibroblasts, and the apoptosis of the cells, respectively. Here  $r_F$  is the cell division rate,  $r_F^{\max}$  is the maximum factor of cell division rate enhancement because of the presence of the chemokines,  $a_c^I$  is the concentration of the chemokines that cause half-maximum enhancement of the cell division rate,  $\kappa_F F$  represents the reduction in the cell division rate because of crowding,  $q$  is a fixed constant,  $k_F$  is the chemokine-dependent cell differentiation rate of fibroblasts into myofibroblasts,  $\delta_N$  is the apoptosis rate of fibroblasts and  $\delta_M$  is the apoptosis rate of myofibroblasts. An important difference between equation (10) and equation (11) is that myofibroblasts only proliferate in the presence of the chemokines. We note that the stimulation of the differentiation of fibroblasts to myofibroblasts by TGF- $\beta$  is only effective in the presence of fibronectin and sufficient mechanical stiffness.

The value of the parameter  $q$  is a consequence of the values of other parameters. Let  $\bar{z} \in \{\bar{c}, \bar{N}, \bar{M}, \bar{\rho}\}$  define the equilibria. Then, if we take  $\bar{M} = 0$  and  $\bar{c} = 0$  as the kinetic equilibrium, then, solving  $R_N = 0$  for  $q$  yields:

$$q = \frac{\log(\delta_N) - \log(r_F(1 - \kappa_F \bar{N}))}{\log(\bar{N})}. \quad (12)$$

It has been shown that myofibroblasts are able to differentiate back to fibroblasts under the influence of Prostaglandin E<sub>2</sub> (PGE<sub>2</sub>) Garrison et al. (2013). Here, we do not take into account the re-differentiation of myofibroblasts to fibroblasts.

### 2.3 Collagen

We assume that secreted collagen is attracted to the ECM instantaneously, hence we assume no active transport for collagen:

$$J_\rho = 0. \quad (13)$$

It is known that both fibroblasts and myofibroblasts secrete collagen. Hence the amount of collagen depends on the number of cells present in the dermal layer. Furthermore, the

secretion rate of collagen is enhanced by the presence of the chemokines. The proteolytic breakdown of collagen is analogous to the breakdown of the chemokines. Hence, we obtain:

$$R_\rho = k_\rho \left[ 1 + \left[ \frac{k_\rho^{\max} c}{a_c^{IV} + c} \right] \right] [N + \eta^I M] - \delta_\rho g(N, M, c, \rho) \rho. \quad (14)$$

Here  $k_\rho$  is the collagen secretion rate,  $k_\rho^{\max}$  is the maximum factor of secretion rate enhancement because of the presence of the chemokines,  $a_c^{IV}$  is the concentration of the chemokines that cause the half-maximum enhancement of the secretion rate and  $\delta_\rho$  is the degradation rate of collagen.

The value of the parameter  $k_\rho$  is a consequence of the values of other parameters. Solving  $R_\rho = 0$  for  $k_\rho$  yields:

$$k_\rho = \delta_\rho \bar{\rho}^2, \quad (15)$$

where we substituted the equilibria with  $\bar{M} = 0$  and  $\bar{c} = 0$ .

## 2.4 The mechanical component

We use a viscoelastic constitutive relation for the mathematical description of the relationship between the Cauchy stress tensor. It is known that myofibroblasts generate an isotropic stress and pull on the ECM. We let this pulling stress be proportional to the product of the cell density of the myofibroblasts and a simple function of the concentration of collagen. Furthermore, we assume that the rate of active change of the effective strain is proportional to the product of the amount of effective strain, the local concentration of the generic MMP, the local concentration of the chemokines, and the inverse of the local concentration of collagen. Taken together, the Cauchy stress, the body force, and the growth tensor,  $\sigma$ ,  $f$ , and  $G$ , respectively, are given by:

$$\sigma = \mu \frac{\partial v}{\partial x} + E \sqrt{\rho} \epsilon, \quad f = \frac{\partial \psi}{\partial x}, \quad G = \alpha \epsilon, \quad \alpha \in \mathbb{R}. \quad (16)$$

Here  $\mu$ ,  $E\sqrt{\rho}$ ,  $\psi$ , respectively, represent the viscosity, the Young's modulus (stiffness) and the total stress generated by the myofibroblasts:

$$\psi = \left[ \frac{\xi M \rho}{R^2 + \rho^2} \right]. \quad (17)$$

Here  $\xi$  represents the generated stress per unit cell density and the inverse of the unit collagen concentration, and  $R$  is a constant.

## 2.5 The displacement velocity and effective strain

We model mass and momentum conservation using equations (3) and (4). In order to incorporate a plastic deformation, we use a tensor-based approach that is also commonly used in the context of growth of tissues (such as tumors). The 'growth' contribution, which in the case of a negative sign models contraction of the tissue, is assumed to be proportional to the product of the cell density of (myo)fibroblasts, and to be a function of

the collagen density. In particular, it is assumed that the tensor for contraction depends on the product of the concentration of the MMPs, the concentration of the chemokines and the reciprocal of the collagen density. To this extent, in line with Koppenol, we use

$$\alpha\epsilon = \zeta \left\{ \frac{[N + \eta^{II}M]c}{1 + a_c^{III}c} \right\} \epsilon. \quad (18)$$

Here  $\zeta$  denotes the rate of morphoelastic change.

## 2.6 Domain of computation and boundary conditions

We define the domain of computation  $\Omega_{x,t}$  by  $(-L, L)$  with  $\partial\Omega_{x,t} = \{-L, L\}$  the boundary points. The dimension  $x$  is in centimeters and  $t$  in days. We impose the following boundary conditions.

For all  $x \in \partial\Omega_{x,t}$  and  $t \geq 0$ :

$$c(x, t) = 0, \quad N(x, t) = \bar{N}, \quad M(x, t) = 0, \quad v(x, t) = 0. \quad (19)$$

For collagen and the effective strain, we do not impose boundary conditions.

Next, we analyze the stability of the model.

## 3 Linear stability of the model

In this section we analyze the stability of the one-dimensional reaction-transport model as well as the stability of the one-dimensional morphoelastic model. In order to invite the reader to continue reading we present the stability analysis of the one-dimensional morphoelastic model first. For this model we consider the stability of the continuous model as well as the stability of the discrete model.

### 3.1 Stability of the one-dimensional morphoelastic model

For simplicity, we consider the equations for the displacement velocity of the dermal layer and the effective strain on the domain  $(0, 1)$ . First we recall the equations:

$$\begin{aligned} \rho_t \left( \frac{\partial v}{\partial t} + 2v \frac{\partial v}{\partial x} \right) - \mu \frac{\partial^2 v}{\partial x^2} - E\sqrt{\rho} \frac{\partial \epsilon}{\partial x} &= f, \\ \frac{\partial \epsilon}{\partial t} + v \frac{\partial \epsilon}{\partial x} + (\epsilon - 1) \frac{\partial v}{\partial x} &= -G, \end{aligned} \quad (20)$$

Here

$$f = \frac{\partial}{\partial x} \left( \frac{\xi M \rho}{R^2 + \rho^2} \right)$$

represents the (temporary) force and

$$G = \alpha\epsilon \quad (21)$$

denotes the permanent growth (or contraction) rate. In case  $\alpha = 0$ , equation (21) models linear visco-elasticity. In this situation, the wound contracts to a certain value, and retracts back to the original configuration. In case  $\alpha > 0$ , equation (21) simulates plasticity, in which the wound contracts and retracts such that at the end of this procedure there exists a permanent deformation.

We analyze perturbations around the equilibria  $v(x, t) = 0$  and

$$\epsilon(x, t) = \begin{cases} \epsilon_0, & \text{if } \alpha = 0, \quad \text{where } \epsilon_0 \in \mathbb{R}_{>0} \\ 0, & \text{if } \alpha > 0. \end{cases}$$

Linearization of the equations (20) around the equilibria gives

$$\begin{aligned} \rho_t \frac{\partial \hat{v}}{\partial t} - \mu \frac{\partial^2 \hat{v}}{\partial x^2} - E \sqrt{\bar{\rho}} \frac{\partial \hat{\epsilon}}{\partial x} &= \hat{f}, \\ \begin{cases} \frac{\partial \hat{\epsilon}}{\partial t} + (\epsilon_0 - 1) \frac{\partial \hat{v}}{\partial x} = 0, & \text{if } \alpha = 0, \\ \frac{\partial \hat{\epsilon}}{\partial t} - \frac{\partial \hat{v}}{\partial x} = -\alpha \hat{\epsilon}, & \text{if } \alpha > 0, \end{cases} \end{aligned} \quad (22)$$

where  $\hat{v}$  and  $\hat{\epsilon}$  are variations around  $v = 0$  and  $\epsilon = \epsilon_0$ , and  $\bar{\rho}$  is the equilibrium density of collagen. In equilibrium, there are no body forces working on the dermal layer, hence  $\hat{f} = 0$ .

### 3.1.1 Stability of the continuous system

We write the variations around the equilibria in terms of a complex Fourier series

$$\hat{v}(x, t) = \sum_{j=-\infty}^{\infty} c_j^v(t) e^{2i\pi j x}, \quad \hat{\epsilon}(x, t) = \sum_{j=-\infty}^{\infty} c_j^\epsilon(t) e^{2i\pi j x}, \quad (23)$$

where  $i$  represents the imaginary unit number and where we use a unit length of the domain of computation for simplicity. Substitution into the equations (22), gives

$$\begin{aligned} \rho_t \sum_{j=-\infty}^{\infty} \dot{c}_j^v(t) e^{2i\pi j x} + \mu \sum_{j=-\infty}^{\infty} (2\pi j)^2 c_j^v(t) e^{2i\pi j x} - i E \sqrt{\bar{\rho}} \sum_{j=-\infty}^{\infty} (2\pi j) c_j^\epsilon(t) e^{2i\pi j x} &= 0, \\ \left\{ \begin{aligned} \sum_{j=-\infty}^{\infty} \dot{c}_j^\epsilon(t) e^{2i\pi j x} + i(\epsilon_0 - 1) \sum_{j=-\infty}^{\infty} (2\pi j) c_j^v(t) e^{2i\pi j x} &= 0, & \text{if } \alpha = 0, \\ \sum_{j=-\infty}^{\infty} \dot{c}_j^\epsilon(t) e^{2i\pi j x} - i \sum_{j=-\infty}^{\infty} (2\pi j) c_j^v(t) e^{2i\pi j x} + \alpha \sum_{j=-\infty}^{\infty} c_j^\epsilon(t) e^{2i\pi j x} &= 0, & \text{if } \alpha > 0. \end{aligned} \right. \end{aligned} \quad (24)$$

We multiply (24) by  $e^{-2i\pi k x}$  and integrate over  $\Omega = (0, 1)$ . Then orthonormality over  $(0, 1)$  implies for the equation for the displacement velocity that

$$\dot{c}_k^v(t) + \frac{(2\pi k)^2 \mu}{\rho_t} c_k^v(t) - i \frac{2\pi k E \sqrt{\bar{\rho}}}{\rho_t} c_k^\epsilon(t) = 0. \quad (25)$$



In case  $\alpha = 0$ , orthonormality over  $(0, 1)$  for the equation for the effective strain implies

$$\dot{c}_k^\epsilon(t) + i 2\pi k(\epsilon_0 - 1)c_k^v(t) = 0. \quad (26)$$

This case represents the situation in which the chemokines disappear from the scar faster than the effective strain stabilizes, and hence there remains an (unknown) effective strain in the scar.

In case  $\alpha > 0$ , the equilibrium  $\epsilon_0 = 0$  holds. Hence orthonormality over  $(0, 1)$  for the equation for the effective strain then implies

$$\dot{c}_k^\epsilon(t) - i 2\pi k c_k^v(t) + \alpha c_k^\epsilon(t) = 0. \quad (27)$$

This case represents the situation in which the effective strain stabilizes faster than the chemokines disappear from the scar.

The following combinations (25)&(26) and (25)&(27) of the above equations are in the form  $y' + Ay = 0$ , with

$$A = \begin{cases} \begin{pmatrix} \frac{(2\pi k)^2 \mu}{\rho_t} & -i \frac{2\pi k E \sqrt{\bar{\rho}}}{\rho_t} \\ i(\epsilon_0 - 1)2\pi k & 0 \end{pmatrix}, & \text{if } \alpha = 0, \\ \begin{pmatrix} \frac{(2\pi k)^2 \mu}{\rho_t} & -i \frac{2\pi k E \sqrt{\bar{\rho}}}{\rho_t} \\ -i2\pi k & \alpha \end{pmatrix}, & \text{if } \alpha > 0. \end{cases}$$

This matrix has the following eigenvalues

$$\lambda_{\pm} = \begin{cases} \frac{(2\pi k)^2 \mu}{2\rho_t} \pm \frac{1}{2} \sqrt{\left(\frac{(2\pi k)^2 \mu}{\rho_t}\right)^2 + 4 \frac{(2\pi k)^2 E \sqrt{\bar{\rho}}}{\rho_t} (\epsilon_0 - 1)}, & \text{if } \alpha = 0, \\ \frac{(2\pi k)^2 \mu}{2\rho_t} + \frac{\alpha}{2} \pm \frac{1}{2} \sqrt{\left(\frac{(2\pi k)^2 \mu}{\rho_t} + \alpha\right)^2 - 4 \frac{(2\pi k)^2}{\rho_t} (\alpha \mu + E \sqrt{\bar{\rho}})}, & \text{if } \alpha > 0. \end{cases} \quad (28)$$

Note that the system is linearly stable if and only if the real part of the eigenvalues is non-negative. In case  $\alpha = 0$ , this implies that linear stability is obtained for  $\epsilon_0 \leq 1$ , else a saddle point problem is obtained if  $\lambda_{\pm} \in \mathbb{R}$ . The eigenvalues are real-valued as long as  $\mu \geq \frac{\sqrt{\rho_t E \sqrt{\bar{\rho}} (1 - \epsilon_0)}}{\pi}$  ( $k = 1$ ). The constant case  $k = 0$  implies  $\lambda_{\pm} = 0$ , which reflects the trivial case in which there are no dynamics. This also implies that  $\epsilon_0 = 0$  is a stable equilibrium state. Next to this, integration of the equations (22) over  $\Omega$ , gives

$$\rho_t \frac{d}{dt} \int_{\Omega} \hat{v} dx = \left[ \mu \frac{\partial \hat{v}}{\partial x} + E \sqrt{\bar{\rho}} \hat{\epsilon} \right]_{-L}^L, \quad (29)$$

$$\frac{d}{dt} \int_{\Omega} \hat{\epsilon} dx + (\epsilon_0 - 1) [\hat{v}]_{-L}^{L_1} = 0 \implies \frac{d}{dt} \int_{\Omega} \hat{\epsilon} dx = 0 \implies \int_{\Omega} \hat{\epsilon} dx = \int_{\Omega} \hat{\epsilon}(0, x) dx.$$

Note that the boundary conditions  $v(-L, t) = v(L, t) = 0$  have been used in the second relation of the above equations. The solution  $\hat{\epsilon}$  to equation (22) converges towards  $\epsilon_0$  under conservation of  $\hat{\epsilon}$  such that  $\int_{\Omega} \hat{\epsilon}(t, x) dx = \int_{\Omega} \hat{\epsilon}(0, x) dx$ . In case  $\alpha > 0$ ,  $\int_{\Omega} \hat{\epsilon}(t, x) dx \longrightarrow 0$ . Furthermore, stability is guaranteed through the fact that

$$4 \frac{(2\pi k)^2}{\rho_t} (\alpha \mu + E \sqrt{\bar{\rho}}) \geq 0, \quad k \in \mathbb{Z}. \quad (30)$$

We summarize these results in Theorem 1.

**Theorem 1.** *Let  $(v, \epsilon)$  satisfy equations (20) under the boundary conditions that  $v = 0$  on the boundaries of open, connected domain  $\Omega \subset \mathbb{R}$ , then*

1. *The equilibria  $(v, \epsilon) = (0, \epsilon_0)$ ,  $\epsilon_0 \in \mathbb{R}$ , are linearly stable if and only if  $\epsilon_0 \leq 1$ ;*
2. *Given  $\epsilon_0 < 1$ , then the eigenvalues are real-valued if and only if*  

$$\mu \geq \frac{\sqrt{\rho_t E \sqrt{\bar{\rho}}(1-\epsilon_0)}}{\pi} |\Omega| \text{ (} k = 1 \text{), where } |\Omega| \text{ denotes the size (measure) of } \Omega;$$
3. *For  $\alpha = 0$ , convergence takes place through  $\int_{\Omega} \hat{\epsilon}(t, x) dx = \int_{\Omega} \hat{\epsilon}(0, x) dx$ ;*
4. *For  $\alpha > 0$ , convergence takes place through  $\int_{\Omega} \hat{\epsilon}(t, x) dx \rightarrow 0$ ;*
5. *For  $\alpha > 0$ , stability is guaranteed given the positivity of the parameters;*

If  $\epsilon_0 < 1$  and if  $\mu < \frac{\sqrt{\rho_t E \sqrt{\bar{\rho}}(1-\epsilon_0)}}{\pi} |\Omega|$  then convergence from variations around  $\epsilon_0$  will occur in a non-monotonic way over time due to the fact that the eigenvalues of the linearized dynamical system are not real-valued.

### 3.1.2 Stability of the discrete system

We apply Von Neumann Stability Analysis for a uniform grid on the following system of equations.

$$\begin{aligned} \frac{\partial v}{\partial t} - \frac{\mu}{\rho_t} \frac{\partial^2 v}{\partial x^2} - \frac{E \sqrt{\bar{\rho}}}{\rho_t} \frac{\partial \epsilon}{\partial x} &= 0, \\ \frac{\partial \epsilon}{\partial t} - \frac{\partial v}{\partial x} + \alpha \epsilon &= 0. \end{aligned} \tag{31}$$

This leads to the following system of block matrices.

$$\frac{\partial}{\partial t} \begin{bmatrix} v \\ \epsilon \end{bmatrix} + \begin{bmatrix} -\frac{\mu}{\rho_t} S & -\frac{E \sqrt{\bar{\rho}}}{\rho_t} C \\ -C & \alpha M \end{bmatrix} \begin{bmatrix} v \\ \epsilon \end{bmatrix} = \underline{0}. \tag{32}$$

Here  $S$ ,  $C$  and  $M$  represent the stiffness matrix ( $v_{xx}$ ), the convection matrix ( $\{v_x, \epsilon_x\}$ ) and the mass matrix ( $\epsilon$ ), respectively. We will show that the eigenvalues of the block matrix have a non-negative real part if  $\alpha > 0$ . This amounts to stability of the equilibria  $v = 0$  and  $\epsilon = 0$ . The *finite difference method* (FDM) gives:

$$\begin{aligned} \lambda v_k &= -\frac{\mu}{\rho_t} \frac{v_{k-1} - 2v_k + v_{k+1}}{h^2} - \frac{E \sqrt{\bar{\rho}}}{\rho_t} \frac{\epsilon_{k+1} - \epsilon_{k-1}}{2h}, \\ \lambda \epsilon_k &= -\frac{v_{k+1} - v_{k-1}}{2h} + \alpha \epsilon_k. \end{aligned} \tag{33}$$

Let

$$(v_k, \epsilon_k) = \sum_{\beta=1}^{n-1} (\hat{v}_{\beta}, \hat{\epsilon}_{\beta}) e^{-2\pi \beta k h i}. \tag{34}$$

Substitution of (34) in equations (33) gives:

$$\begin{aligned}
\lambda \sum_{\beta=1}^{n-1} \hat{v}_{\beta} e^{-2\pi\beta k h i} &= \frac{\mu}{\rho_t h^2} \left[ - \sum_{\beta=1}^{n-1} \hat{v}_{\beta} e^{-2\pi\beta(k-1) h i} + \dots \right. \\
&\quad \left. 2 \sum_{\beta=1}^{n-1} \hat{v}_{\beta} e^{-2\pi\beta k h i} - \sum_{\beta=1}^{n-1} \hat{v}_{\beta} e^{-2\pi\beta(k+1) h i} \right] \\
&\quad - \frac{E\sqrt{\rho}}{2\rho_t h} \left[ \sum_{\beta=1}^{n-1} \hat{\epsilon}_{\beta} e^{-2\pi\beta(k+1) h i} - \sum_{\beta=1}^{n-1} \hat{\epsilon}_{\beta} e^{-2\pi\beta(k-1) h i} \right], \quad (35) \\
\lambda \sum_{\beta=1}^{n-1} \hat{\epsilon}_{\beta} e^{-2\pi\beta k h i} &= -\frac{1}{2h} \left[ \sum_{\beta=1}^{n-1} \hat{v}_{\beta} e^{-2\pi\beta(k+1) h i} - \dots \right. \\
&\quad \left. \sum_{\beta=1}^{n-1} \hat{v}_{\beta} e^{-2\pi\beta(k-1) h i} \right] + \alpha \sum_{\beta=1}^{n-1} \hat{\epsilon}_{\beta} e^{-2\pi\beta k h i}.
\end{aligned}$$

This must be true for arbitrary  $\{v_{\beta}, \epsilon_{\beta}\}$ , hence each factor following  $\{v_{\beta}, \epsilon_{\beta}\}$  in the sum should be zero. Subdivision by  $e^{2\pi\beta k h i}$  results in

$$\begin{aligned}
\lambda \hat{v}_{\beta} &= \frac{\mu}{\rho_t h^2} \left[ -\hat{v}_{\beta} e^{2\pi\beta h i} + 2\hat{v}_{\beta} - \hat{v}_{\beta} e^{-2\pi\beta h i} \right] + \frac{E\sqrt{\rho}}{2\rho_t h} \left[ -\hat{\epsilon}_{\beta} e^{-2\pi\beta h i} + \hat{\epsilon}_{\beta} e^{2\pi\beta h i} \right], \quad (36) \\
\lambda \hat{\epsilon}_{\beta} &= \frac{1}{2h} \left[ -\hat{v}_{\beta} e^{-2\pi\beta h i} + \hat{v}_{\beta} e^{2\pi\beta h i} \right] + \alpha \hat{\epsilon}_{\beta}.
\end{aligned}$$

Using Euler's formula we get

$$\begin{aligned}
\lambda \hat{v}_{\beta} &= \frac{\mu}{\rho_t h^2} [2 - 2\cos(2\pi\beta h)] \hat{v}_{\beta} + \frac{E\sqrt{\rho}i}{\rho_t h} \sin(2\pi\beta h) \hat{\epsilon}_{\beta}, \\
\lambda \hat{\epsilon}_{\beta} &= \frac{i}{h} \sin(2\pi\beta h) \hat{v}_{\beta} + \alpha \hat{\epsilon}_{\beta}. \quad (37)
\end{aligned}$$

Solving for the second equation in (37) yields

$$\hat{\epsilon}_{\beta} = \frac{i \sin(2\pi\beta h) \hat{v}_{\beta}}{h(\lambda - \alpha)}. \quad (38)$$

Substitution for  $\hat{\epsilon}_{\beta}$  in the first equation in (37) yields after multiplication by  $\frac{\lambda - \alpha}{\hat{v}_{\beta}}$  and rearrangement for  $\lambda$ :

$$\lambda^2 - \left[ \alpha + \frac{4\mu}{\rho_t h^2} \sin^2(\pi\beta h) \right] \lambda + \alpha \frac{4\mu}{\rho_t h^2} \sin^2(\pi\beta h) + \frac{E\sqrt{\rho}}{\rho_t h^2} \sin^2(2\pi\beta h) = 0. \quad (39)$$

Solving (39) yields

$$\lambda_{\pm} = \frac{1}{2} \left[ \alpha + \frac{4\mu}{\rho_t h^2} \sin^2(\pi\beta h) \right] \pm \frac{1}{2} \sqrt{\left[ \alpha + \frac{4\mu}{\rho_t h^2} \sin^2(\pi\beta h) \right]^2 - 4 \left[ \alpha \frac{4\mu}{\rho_t h^2} \sin^2(\pi\beta h) + \frac{E\sqrt{\rho}}{\rho_t h^2} \sin^2(2\pi\beta h) \right]}. \quad (40)$$

Since

$$4 \left[ \alpha \frac{4\mu}{\rho_t h^2} \sin^2(\pi\beta h) + \frac{E\sqrt{\rho}}{\rho_t h^2} \sin^2(2\pi\beta h) \right] \geq 0, \quad (41)$$

stability is guaranteed for all  $h \in \mathbb{R}_{>0}$ .

There exists a consistency between the continuous stability criteria and the discrete stability criteria. We show this consistency by writing  $\sin^2(x)$  as a Taylor series. Substitution into equation (40) yields:

$$\frac{1}{2} \left[ \alpha + \frac{\mu}{\rho_t} (2\pi\beta)^2 + \mathcal{O}(h^2) \right] \pm \frac{1}{2} \sqrt{\left[ \alpha + \frac{\mu}{\rho_t} (2\pi\beta)^2 + \mathcal{O}(h^2) \right]^2 - 4 \left[ \alpha \frac{\mu}{\rho_t} (2\pi\beta)^2 + \frac{E\sqrt{\rho}}{\rho_t} (2\pi\beta)^2 + \mathcal{O}(h^2) \right]}. \quad (42)$$

Comparison to the second equation of (28)

$$\frac{1}{2} \left[ \alpha + \frac{\mu}{\rho_t} (2\pi k)^2 \right] \pm \frac{1}{2} \sqrt{\left[ \alpha + \frac{\mu}{\rho_t} (2\pi k)^2 \right]^2 - 4 \left[ \alpha \frac{\mu}{\rho_t} (2\pi k)^2 + \frac{E\sqrt{\rho}}{\rho_t} (2\pi k)^2 \right]}$$

yields a difference in eigenvalues of order  $\mathcal{O}(h^2)$ . We summarize the results in Theorem 2.

**Theorem 2.** *Let  $(v, \epsilon)$  satisfy equations (31) under the boundary conditions that  $v = 0$  on the boundaries of open, connected domain  $\Omega \subset \mathbb{R}$ . Then the equilibrium  $(v, \epsilon) = (0, 0)$  is linearly stable for the semi-discrete problem that makes use of divided difference approximations. The truncation error is  $\mathcal{O}(h^2)$ .*

**Corollary 1.** *Let  $(v, \epsilon)$  satisfy equations (31) under the boundary conditions that  $v = 0$  on the boundaries of open, connected domain  $\Omega \subset \mathbb{R}$ . Then the equilibria are unconditionally stable for the trapezoid rule and the Euler backward method. Furthermore, the Euler backward method is A-stable.*

Next, we present the stability analysis of the 1D reaction-transport model.

### 3.2 Stability of the one-dimensional reaction-transport model

We analyze stability for the one-dimensional reaction-transport model on  $(0, 1)$ . We consider the equations for the chemokines, the fibroblasts, the myofibroblasts and collagen,

independent of the displacement velocity of the dermal layer (i.e.,  $v = 0$ ). First we recall the reaction-transport equation:

$$\frac{\partial z}{\partial t} = -\frac{\partial J_z}{\partial x} + R_z, \quad z \in \{c, N, M, \rho\}. \quad (43)$$

We analyze perturbations around the equilibria  $\bar{z} = \{0, \bar{N}, 0, \bar{\rho}\}$  for the case that there are no forces and no deformation, that is  $v = 0$ . Linearization of equation (43) around the equilibria and  $v = 0$  gives

$$\begin{aligned} \frac{\partial \hat{c}}{\partial t} - D_c \frac{\partial^2 \hat{c}}{\partial x^2} + \left[ \delta_c \bar{\rho} - \frac{k_c}{a_c^{II}} \right] \bar{N} \hat{c} &= 0, \\ \frac{\partial \hat{N}}{\partial t} - D_F \bar{N} \frac{\partial^2 \hat{N}}{\partial x^2} + \chi_F \bar{N} \frac{\partial^2 \hat{c}}{\partial x^2} + [\delta_N - r_F(1 - \kappa_F \bar{N}) \bar{N}^q] \hat{N} + k_F \bar{N} \hat{c} &= 0, \\ \frac{\partial \hat{M}}{\partial t} - D_F \bar{N} \frac{\partial^2 \hat{M}}{\partial x^2} + \delta_M \hat{M} - k_F \bar{N} \hat{c} &= 0, \\ \frac{\partial \hat{\rho}}{\partial t} - k_\rho \hat{N} - k_\rho \eta^I \hat{M} + \delta_\rho \bar{N} \bar{\rho} \hat{\rho} &= 0. \end{aligned} \quad (44)$$

We will analyze stability for the continuous system as well as the discrete system using these linearized equations.

### 3.3 Stability of the continuous system

We write the variations in terms of a complex Fourier series, that is, we set

$$\begin{aligned} \hat{c}(x, t) &= \sum_{j=-\infty}^{\infty} c_j^c(t) e^{2i\pi j x}, & \hat{\rho}(x, t) &= \sum_{j=-\infty}^{\infty} c_j^\rho(t) e^{2i\pi j x}, \\ \hat{N}(x, t) &= \sum_{j=-\infty}^{\infty} c_j^N(t) e^{2i\pi j x}, & \hat{M}(x, t) &= \sum_{j=-\infty}^{\infty} c_j^M(t) e^{2i\pi j x}, \end{aligned} \quad (45)$$

where  $i$  represents the imaginary unit number and where we use a unit length of the domain of computation for simplicity. Substitution of the variations into equations (44) gives

$$\begin{aligned} \sum_{j=-\infty}^{\infty} \dot{v}_j^c(t) e^{2i\pi j x} + D_c \sum_{j=-\infty}^{\infty} (2\pi j)^2 c_j^c(t) e^{2i\pi j x} \\ + \left[ \delta_c \bar{\rho} - \frac{k_c}{a_c^{II}} \right] \bar{N} \sum_{j=-\infty}^{\infty} c_j^c(t) e^{2i\pi j x} = 0, \end{aligned} \quad (46)$$

$$\begin{aligned}
& \sum_{j=-\infty}^{\infty} \dot{v}_j^N(t) e^{2i\pi jx} + D_F \bar{N} \sum_{j=-\infty}^{\infty} (2\pi j)^2 c_j^N(t) e^{2i\pi jx} \\
& - \chi_F \bar{N} \sum_{j=-\infty}^{\infty} (2\pi j)^2 c_j^c(t) e^{2i\pi jx} + [\delta_N - r_F(1 - \kappa_F \bar{N}) \bar{N}^q] \sum_{j=-\infty}^{\infty} c_j^N(t) e^{2i\pi jx} \\
& + k_F \bar{N} \sum_{j=-\infty}^{\infty} c_j^c(t) e^{2i\pi jx} = 0, \quad (47)
\end{aligned}$$

$$\begin{aligned}
& \sum_{j=-\infty}^{\infty} \dot{v}_j^M(t) e^{2i\pi jx} + D_F \bar{N} \sum_{j=-\infty}^{\infty} (2\pi j)^2 c_j^M(t) e^{2i\pi jx} \\
& - k_F \bar{N} \sum_{j=-\infty}^{\infty} c_j^c(t) e^{2i\pi jx} + \delta_M \sum_{j=-\infty}^{\infty} c_j^M(t) e^{2i\pi jx} = 0, \quad (48)
\end{aligned}$$

$$\begin{aligned}
& \sum_{j=-\infty}^{\infty} \dot{v}_j^\rho(t) e^{2i\pi jx} - k_\rho \sum_{j=-\infty}^{\infty} c_j^N(t) e^{2i\pi jx} - k_\rho \eta^I \sum_{j=-\infty}^{\infty} c_j^M(t) e^{2i\pi jx} \\
& + \delta_M \bar{N} \bar{\rho} \sum_{j=-\infty}^{\infty} c_j^\rho(t) e^{2i\pi jx} = 0. \quad (49)
\end{aligned}$$

Orthonormality over  $\Omega = (0, 1)$  implies after multiplication by  $e^{-2i\pi kx}$  and integration over  $\Omega$  that

$$\dot{v}_k^c(t) + D_c(2\pi k)^2 c_k^c(t) + \left[ \delta_c \bar{\rho} - \frac{k_c}{a_{II}^I} \right] \bar{N} c_k^c(t) = 0, \quad (50)$$

$$\begin{aligned}
\dot{v}_k^N(t) + [D_F \bar{N} (2\pi k)^2 + \delta_N - r_F(1 - \kappa_F \bar{N}) \bar{N}^q] c_k^N(t) \\
+ (k_F - \chi_F (2\pi k)^2) \bar{N} c_k^c(t) = 0, \quad (51)
\end{aligned}$$

$$\dot{v}_k^M(t) + D_F \bar{N} (2\pi k)^2 c_k^M(t) - k_F \bar{N} c_k^c(t) + \delta_M c_k^M(t) = 0, \quad (52)$$

$$\dot{v}_k^\rho(t) - k_\rho c_k^N(t) - k_\rho \eta^I c_k^M(t) + \delta_M \bar{N} \bar{\rho} c_k^\rho(t) = 0. \quad (53)$$

After a small rearrangement the equations (50)-(53) are in the form  $y' + By = 0$ , with

$$B = \begin{pmatrix} B_{11} & 0 & B_{13} & 0 \\ 0 & B_{22} & B_{23} & 0 \\ 0 & 0 & B_{33} & 0 \\ B_{41} & B_{42} & 0 & B_{44} \end{pmatrix}. \quad (54)$$

The eigenvalues of the matrix  $B$  are found on the diagonal:

$$\begin{aligned}
B_{11} &= (2\pi k)^2 D_F \bar{N} + \delta_N - r_F(1 - \kappa_F \bar{N}) \bar{N}^q, \\
B_{22} &= (2\pi k)^2 D_F \bar{N} + \delta_M, \\
B_{33} &= (2\pi k)^2 D_c + \delta_c \bar{N} \bar{\rho} - \frac{k_c \bar{N}}{a_c^{II}}, \\
B_{44} &= \delta_\rho \bar{N} \bar{\rho}.
\end{aligned} \tag{55}$$

The second and fourth eigenvalues meet the stability condition  $\text{Re}(\lambda(B)) \geq 0$  independent of the chosen values for the parameters given that the parameters are positive. Furthermore, given equation (12), we have  $\delta_N = r_F(1 - \kappa_F \bar{N}) \bar{N}^q$ , which implies that the first eigenvalue also meets the stability condition. However, it should be noted that the behavior of the non-linear system is uncertain because  $B_{11} = 0$  if  $k = 0$ . Taken together, stability for the undamaged state is guaranteed under only one condition. We formalize this result in Theorem 3.

**Theorem 3.** *Let  $z$ ,  $z \in \{c, N, M, \rho\}$  satisfy*

$$\frac{\partial z}{\partial t} = -\frac{\partial J_z}{\partial x} + R_z,$$

*and  $(c, N, M, \rho) = (0, \bar{N}, 0, \bar{\rho})$ ,  $\{\bar{N}, \bar{\rho}\} \in \mathbb{R}_{>0}$  on the boundaries of open, connected domain  $\Omega \subset \mathbb{R}$ . Let  $J_z$ ,  $R_z$ ,  $z \in \{c, N, M, \rho\}$  as in equations (5)-(11). Then the equilibria  $(c, N, M, \rho) = (0, \bar{N}, 0, \bar{\rho})$ ,  $\{\bar{N}, \bar{\rho}\} \in \mathbb{R}_{>0}$ , are linearly stable if and only if*

$$(2\pi k)^2 D_c + \delta_c \bar{N} \bar{\rho} \geq \frac{k_c \bar{N}}{a_c^{II}}, \tag{56}$$

*for each  $k \in \mathbb{Z}$ .*

*Note that*

$$\delta_c \geq \frac{k_c}{a_c^{II} \bar{\rho}}, \tag{57}$$

*for  $k = 0$  (constant states). Hence, if constant perturbations are stable, then wave-like perturbations are stable. In case  $\delta_c$  is not large enough, fast oscillating perturbations will vanish, while slow oscillating perturbations will not vanish and can amplify.*

### 3.4 Stability of the discrete system

We apply Von Neumann Stability Analysis on equations (44). The *finite difference method* (FDM) gives:

$$\begin{aligned}
\lambda c_k &= -D_c \frac{c_{k-1} - 2c_k + c_{k+1}}{h^2} + \left[ \delta_c \bar{\rho} - \frac{k_c}{a_c^{II}} \right] \bar{N} c_k, \\
\lambda N_k &= -D_F \bar{N} \frac{N_{k-1} - 2N_k + N_{k+1}}{h^2} + \chi_F \bar{N} \frac{c_{k-1} - 2c_k + c_{k+1}}{h^2} \\
&\quad + [\delta_N - r_F(1 - \kappa_F \bar{N}) \bar{N}^q] N_k + k_F \bar{N} c_k, \\
\lambda M_k &= -D_F \bar{N} \frac{M_{k-1} - 2M_k + M_{k+1}}{h^2} + \delta_M M_k - k_F \bar{N} c_k, \\
\lambda \rho_k &= -k_\rho N_k - k_\rho \eta^I M_k + \delta_\rho \bar{N} \bar{\rho} \rho_k.
\end{aligned} \tag{58}$$

Let

$$(c_k, N_k, M_k, \rho_k) = \sum_{\beta=1}^{n-1} (\hat{c}_\beta, \hat{N}_\beta, \hat{M}_\beta, \hat{\rho}_\beta) e^{-2\pi\beta k h i}. \tag{59}$$

Substitution of (59) in equations (58) gives:

$$\begin{aligned}
\lambda \sum_{\beta=1}^{n-1} \hat{c}_\beta e^{-2\pi\beta k h i} &= -\frac{D_c}{h^2} \left[ \sum_{\beta=1}^{n-1} \hat{c}_\beta e^{-2\pi\beta(k-1)h i} - 2 \sum_{\beta=1}^{n-1} \hat{c}_\beta e^{-2\pi\beta k h i} \right. \\
&\quad \left. + \sum_{\beta=1}^{n-1} \hat{c}_\beta e^{-2\pi\beta(k+1)h i} \right] \\
&\quad + \left[ \delta_c \bar{\rho} - \frac{k_c}{a_c^{II}} \right] \bar{N} \sum_{\beta=1}^{n-1} \hat{c}_\beta e^{-2\pi\beta k h i}, \tag{60}
\end{aligned}$$

$$\begin{aligned}
\lambda \sum_{\beta=1}^{n-1} \hat{N}_\beta e^{-2\pi\beta k h i} &= -\frac{D_F \bar{N}}{h^2} \left[ \sum_{\beta=1}^{n-1} \hat{N}_\beta e^{-2\pi\beta(k-1)h i} \right. \\
&\quad \left. - 2 \sum_{\beta=1}^{n-1} \hat{N}_\beta e^{-2\pi\beta k h i} + \sum_{\beta=1}^{n-1} \hat{N}_\beta e^{-2\pi\beta(k+1)h i} \right] \\
&\quad + \frac{\chi_F \bar{N}}{h^2} \left[ \sum_{\beta=1}^{n-1} \hat{c}_\beta e^{-2\pi\beta(k-1)h i} - 2 \sum_{\beta=1}^{n-1} \hat{c}_\beta e^{-2\pi\beta k h i} + \sum_{\beta=1}^{n-1} \hat{c}_\beta e^{-2\pi\beta(k+1)h i} \right] \\
&\quad + [\delta_N - r_F(1 - \kappa_F \bar{N}) \bar{N}^q] \sum_{\beta=1}^{n-1} \hat{N}_\beta e^{-2\pi\beta k h i} + k_F \bar{N} \sum_{\beta=1}^{n-1} \hat{c}_\beta e^{-2\pi\beta k h i}, \tag{61}
\end{aligned}$$



$$\begin{aligned}
\lambda \sum_{\beta=1}^{n-1} \hat{M}_\beta e^{-2\pi\beta k h i} &= -\frac{D_F \bar{N}}{h^2} \left[ \sum_{\beta=1}^{n-1} \hat{M}_\beta e^{-2\pi\beta(k-1) h i} \right. \\
&\quad \left. - 2 \sum_{\beta=1}^{n-1} \hat{M}_\beta e^{-2\pi\beta k h i} + \sum_{\beta=1}^{n-1} \hat{M}_\beta e^{-2\pi\beta(k+1) h i} \right] \\
&\quad + \delta_M \sum_{\beta=1}^{n-1} \hat{M}_\beta e^{-2\pi\beta k h i} - k_F \bar{N} \sum_{\beta=1}^{n-1} \hat{c}_\beta e^{-2\pi\beta k h i}, \quad (62)
\end{aligned}$$

$$\begin{aligned}
\lambda \sum_{\beta=1}^{n-1} \hat{\rho}_\beta e^{-2\pi\beta k h i} &= -k_\rho \sum_{\beta=1}^{n-1} \hat{N}_\beta e^{-2\pi\beta k h i} - k_\rho \eta^I \sum_{\beta=1}^{n-1} \hat{M}_\beta e^{-2\pi\beta k h i} \\
&\quad + \delta_\rho \bar{N} \bar{\rho} \sum_{\beta=1}^{n-1} \hat{\rho}_\beta e^{-2\pi\beta k h i}. \quad (63)
\end{aligned}$$

This must be true for arbitrary  $\{c_\beta, N_\beta, M_\beta, \rho_\beta\}$ , hence each factor following  $\{c_\beta, N_\beta, M_\beta, \rho_\beta\}$  in the sum should be zero. Subdivision by  $e^{-2\pi\beta k h i}$  results in

$$\begin{aligned}
\lambda \hat{c}_\beta &= -\frac{D_c}{h^2} \left[ e^{2\pi\beta h i} - 2 + e^{-2\pi\beta h i} \right] \hat{c}_\beta + \left[ \delta_c \bar{\rho} - \frac{k_c}{a_c^{II}} \right] \bar{N} \hat{c}_\beta, \\
\lambda \hat{N}_\beta &= -\frac{D_F \bar{N}}{h^2} \left[ e^{2\pi\beta h i} - 2 + e^{-2\pi\beta h i} \right] \hat{N}_\beta + \frac{\chi_F \bar{N}}{h^2} \left[ e^{2\pi\beta h i} - 2 + e^{-2\pi\beta h i} \right] \hat{c}_\beta \\
&\quad + [\delta_N - r_F(1 - \kappa_F \bar{N}) \bar{N}^q] \hat{N}_\beta + k_F \bar{N} \hat{c}_\beta, \\
\lambda \hat{M}_\beta &= -\frac{D_F \bar{N}}{h^2} \left[ e^{2\pi\beta h i} - 2 + e^{-2\pi\beta h i} \right] \hat{M}_\beta + \delta_M \hat{M}_\beta - k_F \bar{N} \hat{c}_\beta, \\
\lambda \rho_k &= -k_\rho \hat{N}_\beta - k_\rho \eta^I \hat{M}_\beta + \delta_\rho \bar{N} \bar{\rho} \hat{\rho}_\beta.
\end{aligned} \quad (64)$$

Using Euler's formula and  $2 - 2\cos(2\pi\beta h) = 4\sin^2(\pi\beta h)$  we get

$$\begin{aligned}
\lambda \hat{c}_\beta &= \frac{D_c}{h^2} 4\sin^2(\pi\beta h) \hat{c}_\beta + \left[ \delta_c \bar{\rho} - \frac{k_c}{a_c^{II}} \right] \bar{N} \hat{c}_\beta, \\
\lambda \hat{N}_\beta &= \frac{D_F \bar{N}}{h^2} 4\sin^2(\pi\beta h) \hat{N}_\beta - \frac{\chi_F \bar{N}}{h^2} 4\sin^2(\pi\beta h) \hat{c}_\beta \\
&\quad + [\delta_N - r_F(1 - \kappa_F \bar{N}) \bar{N}^q] \hat{N}_\beta + k_F \bar{N} \hat{c}_\beta, \\
\lambda \hat{M}_\beta &= \frac{D_F \bar{N}}{h^2} 4\sin^2(\pi\beta h) \hat{M}_\beta + \delta_M \hat{M}_\beta - k_F \bar{N} \hat{c}_\beta, \\
\lambda \rho_k &= -k_\rho \hat{N}_\beta - k_\rho \eta^I \hat{M}_\beta + \delta_\rho \bar{N} \bar{\rho} \hat{\rho}_\beta.
\end{aligned} \quad (65)$$

Above equations (65) are in the form  $\lambda \mathbf{z} = C \mathbf{z}$ , with

$$C = \begin{pmatrix} C_{11} & 0 & C_{13} & 0 \\ 0 & C_{22} & C_{23} & 0 \\ 0 & 0 & C_{33} & 0 \\ C_{41} & C_{42} & 0 & C_{44} \end{pmatrix}. \quad (66)$$

Again, the eigenvalues of the matrix  $C$  are found on the main diagonal:

$$\begin{aligned}\lambda_N &= \frac{D_F \bar{N}}{h^2} 4 \sin^2(\pi \beta h) + [\delta_N - r_F(1 - \kappa_F \bar{N}) \bar{N}^q], \\ \lambda_M &= \frac{D_F \bar{N}}{h^2} 4 \sin^2(\pi \beta h) + \delta_M, \\ \lambda_c &= \frac{D_c}{h^2} 4 \sin^2(\pi \beta h) + \left[ \delta_c \bar{\rho} - \frac{k_c}{a_c^{II}} \right] \bar{N}, \\ \lambda_\rho &= \delta_\rho \bar{N} \bar{\rho}.\end{aligned}\tag{67}$$

Given equation (12), the first, second and fourth eigenvalues meet the stability condition  $\text{Re}(\lambda(C)) \geq 0$  independent of the chosen values for the parameters given that the parameters are positive. Hence, stability is guaranteed for only one condition.

There is a consistency between the eigenvalues of the discrete model and the eigenvalues of the continuous model. After writing the sine as a Taylor series, substitution in the third equation of (67) yields:

$$\lambda_c = D_c [(2\pi\beta)^2 + \mathcal{O}(h^2)] + \left[ \delta_c \bar{\rho} - \frac{k_c}{a_c^{II}} \right] \bar{N}.\tag{68}$$

Comparison with the third equation of (55) show a difference of order  $\mathcal{O}(h^2)$ . We formalize the results in Theorem 4.

**Theorem 4.** *Let  $z, z \in \{c, N, M, \rho\}$  satisfy*

$$\frac{\partial z}{\partial t} = -\frac{\partial J_z}{\partial x} + R_z,$$

*and  $(c, N, M, \rho) = (0, \bar{N}, 0, \bar{\rho})$ ,  $\{\bar{N}, \bar{\rho}\} \in \mathbb{R}_{>0}$  on the boundaries of open, connected domain  $\Omega \subset \mathbb{R}$ . Let  $J_z, R_z, z \in \{c, N, M, \rho\}$  as in equations (5)-(11). Then, for the finite difference method with element length  $h$ , the equilibria  $(c, N, M, \rho) = (0, \bar{N}, 0, \bar{\rho})$ ,  $\{\bar{N}, \bar{\rho}\} \in \mathbb{R}_{>0}$ , are linearly stable if and only if*

$$\frac{D_c}{h^2} 4 \sin^2(\pi \beta h) + \delta_c \bar{\rho} \bar{N} \geq \frac{k_c}{a_c^{II}} \bar{N},\tag{69}$$

*for each  $\beta \in \mathbb{Z}$  and  $h > 0$ . The truncation error is of order  $\mathcal{O}(h^2)$ .*

Next, we describe the numerical method we use to validate the stability constraints.

## 4 Numerical method for validation

We approximate the solution to the model equations by the finite-element method using linear basis functions. For more information about this method we refer to Van Kan et al. (2014). We divide the domain of computation in  $n$  equidistant elements, each with length  $|e_p| = x_{i+1} - x_i$ .

#### 4.1 Numerical method for the one-dimensional mechanical model

Multiplication of the first and third equations (22) by a test function, integration over the domain of computation (integration by parts) and the application of the Gauss' theorem results in:

$$\begin{aligned} \rho_t \int_{\Omega} \frac{\partial \hat{v}}{\partial t} \varphi \, dx + \int_{\Omega} \left\{ \mu \frac{\partial \hat{v}}{\partial x} \frac{d\varphi}{dx} + E \sqrt{\bar{\rho}} \hat{\epsilon} \frac{d\varphi}{dx} \right\} dx &= 0, \\ \int_{\Omega} \frac{\partial \hat{\epsilon}}{\partial t} \varphi \, dx + \int_{\Omega} \left\{ \hat{v} \frac{d\varphi}{dx} + \alpha \hat{\epsilon} \varphi \right\} dx &= 0. \end{aligned} \quad (70)$$

After application of the Galerkin method, where

$$\hat{v}(x, t) \approx \sum_{j=1}^n c_j^v(t) \varphi_j(x) \quad \text{and} \quad \hat{\epsilon}(x, t) \approx \sum_{j=1}^n c_j^\epsilon(t) \varphi_j(x), \quad (71)$$

one gets

$$\begin{aligned} \rho_t \sum_{j=1}^n \mathcal{M}_{ij} \frac{dc_j^v(t)}{dt} + \sum_{j=1}^n \mathcal{S}_{ij}^{vv} c_j^v(t) + \sum_{j=1}^n \mathcal{S}_{ij}^{v\epsilon} c_j^\epsilon(t) &= 0, \\ \sum_{j=1}^n \mathcal{M}_{ij} \frac{dc_j^\epsilon(t)}{dt} + \sum_{j=1}^n \mathcal{S}_{ij}^{\epsilon v} c_j^v(t) + \sum_{j=1}^n \mathcal{S}_{ij}^{\epsilon\epsilon} c_j^\epsilon(t) &= 0, \end{aligned} \quad (72)$$

or more shortly

$$\begin{aligned} \rho_t \mathcal{M} \frac{d\underline{c}^v(t)}{dt} + \mathcal{S}^{vv} \underline{c}^v(t) + \mathcal{S}^{v\epsilon} \underline{c}^\epsilon(t) &= 0, \\ \mathcal{M} \frac{d\underline{c}^\epsilon(t)}{dt} + \mathcal{S}^{\epsilon v} \underline{c}^v(t) + \mathcal{S}^{\epsilon\epsilon} \underline{c}^\epsilon(t) &= 0. \end{aligned} \quad (73)$$

We solve the system using backward Euler time integration, that is

$$\begin{bmatrix} \hat{v}^{t+\delta t} \\ \hat{\epsilon}^{t+\delta t} \end{bmatrix} = \begin{bmatrix} \rho_t \mathcal{M} + \mathcal{S}^{vv} \delta t & \mathcal{S}^{v\epsilon} \delta t \\ \mathcal{S}^{\epsilon v} \delta t & \mathcal{M} + \mathcal{S}^{\epsilon\epsilon} \delta t \end{bmatrix}^{-1} \begin{bmatrix} \rho_t \mathcal{M} \hat{v}^t \\ \mathcal{M} \hat{\epsilon}^t \end{bmatrix}. \quad (74)$$

The mass matrix and stiffness matrices are given by

$$\begin{aligned} \mathcal{M}_{ij} &= \frac{|e_p|}{6} \begin{bmatrix} 2 & 1 \\ 1 & 2 \end{bmatrix}, \\ \mathcal{S}_{ij}^{vv} &= \frac{\mu}{|e_p|} \begin{bmatrix} 1 & -1 \\ -1 & 1 \end{bmatrix}, \quad \mathcal{S}_{ij}^{v\epsilon} = \frac{E \sqrt{\bar{\rho}}}{2} \begin{bmatrix} -1 & -1 \\ 1 & 1 \end{bmatrix}, \\ \mathcal{S}_{ij}^{\epsilon v} &= \frac{1}{2} \begin{bmatrix} -1 & -1 \\ 1 & 1 \end{bmatrix}, \quad \mathcal{S}_{ij}^{\epsilon\epsilon} = \alpha \frac{|e_p|}{6} \begin{bmatrix} 2 & 1 \\ 1 & 2 \end{bmatrix}. \end{aligned} \quad (75)$$

## 4.2 Numerical method for the one-dimensional transport model

Multiplication of equations (43) by a test function, integration over the domain of computation (integration by parts), the application of the Gauss' theorem, and the application of the Leibniz-Reynold's transport theorem results in:

$$\begin{aligned} \frac{d}{dt} \int_{\Omega_{x,t}} \varphi c \, d\Omega_{x,t} = \\ \int_{\Omega_{x,t}} -D_c \frac{d\varphi}{dx} \frac{\partial c}{\partial x} + \varphi \left( k_c \left[ \frac{c}{a_c^{II} + c} \right] [N + \eta^I M] - \delta_c \frac{[N + \eta^{II} M] \rho}{1 + a_c^{III} c} c \right) d\Omega_{x,t}, \end{aligned} \quad (76)$$

$$\begin{aligned} \frac{d}{dt} \int_{\Omega_{x,t}} \varphi N \, d\Omega_{x,t} = \int_{\Omega_{x,t}} \frac{d\varphi}{dx} \left( -D_F F \frac{\partial N}{\partial x} + \chi_F N \frac{\partial c}{\partial x} \right) \\ + \varphi \left( r_F \left[ 1 + \frac{r_F^{\max} c}{a_c^I + c} \right] [1 - \kappa_F F] N^{1+q} - k_F c N - \delta_N N \right) d\Omega_{x,t}, \end{aligned} \quad (77)$$

$$\begin{aligned} \frac{d}{dt} \int_{\Omega_{x,t}} \varphi M \, d\Omega_{x,t} = \int_{\Omega_{x,t}} \frac{d\varphi}{dx} \left( -D_F F \frac{\partial M}{\partial x} + \chi_F M \frac{\partial c}{\partial x} \right) \\ + \varphi \left( r_F \left\{ \frac{[1 + r_F^{\max}] c}{a_c^I + c} \right\} [1 - \kappa_F F] M^{1+q} + k_F c N - \delta_M M \right) d\Omega_{x,t}, \end{aligned} \quad (78)$$

$$\begin{aligned} \frac{d}{dt} \int_{\Omega_{x,t}} \varphi \rho \, d\Omega_{x,t} = \\ \int_{\Omega_{x,t}} \varphi \left( k_\rho \left\{ 1 + \left[ \frac{k_\rho^{\max} c}{a_c^{IV} + c} \right] \right\} [N + \eta^I M] - \delta_\rho \frac{[N + \eta^{II} M] \rho}{1 + a_c^{III} c} \rho \right) d\Omega_{x,t}. \end{aligned} \quad (79)$$

After application of the Galerkin method, where

$$\begin{aligned} \hat{c}(x, t) &\approx \sum_{j=1}^n c_j^c(t) \varphi_j(x), & \hat{N}(x, t) &\approx \sum_{j=1}^n c_j^N(t) \varphi_j(x), \\ \hat{M}(x, t) &\approx \sum_{j=1}^n c_j^M(t) \varphi_j(x), & \hat{\rho}(x, t) &\approx \sum_{j=1}^n c_j^\rho(t) \varphi_j(x), \end{aligned} \quad (80)$$

one gets

$$\begin{aligned} \mathcal{M} \frac{d\underline{c}^c(t)}{dt} + \mathcal{S}^c \underline{c}^c(t) &= 0, \\ \mathcal{M} \frac{d\underline{c}^N(t)}{dt} + \mathcal{S}^N \underline{c}^N(t) &= 0, \\ \mathcal{M} \frac{d\underline{c}^M(t)}{dt} + \mathcal{S}^M \underline{c}^v(t) &= \mathcal{F}^M, \\ \mathcal{M} \frac{d\underline{c}^\rho(t)}{dt} + \mathcal{S}^\rho \underline{c}^v(t) &= \mathcal{F}^\rho. \end{aligned} \quad (81)$$

We solve equations (81) using backward Euler time integration and we use a monolithic approach with inner Picard iterations to account for the non-linearity of the equations. The stiffness matrices and element vectors are found in the Appendix. To avoid loss of monotonicity (i.e. oscillations), we use the process called mass lumping. Hence the mass matrix becomes

$$\mathcal{M}_{lump}^{e_p} = \frac{|e_p|}{2} \begin{bmatrix} 1 & 0 \\ 0 & 1 \end{bmatrix}. \quad (82)$$

Next, we discuss the results of the numerical validation.

## 5 Results

### 5.1 Validation of the stability of the one-dimensional mechanical model

We validate the stability of the model by ranging parameters. First, we fix the following parameters: the total mass density  $\rho_t = 1.09$ , the collagen equilibrium density  $\bar{\rho} = 0.1125$ , and the rate of morphoelastic change  $\alpha = 0.22$ . We vary the viscosity parameter using two levels (1 and 10) and the number of waves  $k$  using four levels (1, 2, 3 and 10). We use 1000 elements to divide the domain of computation between 0 and 5. The initial amplitudes of the displacement velocity and effective strain is 1. We simulate the evolution of the displacement velocity and effective strain after the initial density is perturbed using sine functions. We show the most significant simulation results.

Figures 1 and 2 show the stable evolution of the displacement velocity and effective strain for different parameters. Since  $\alpha > 0$ , equation (30) guarantees the stability.

In case the viscosity is high (Figure 1), all the positive values of the displacement velocity directly decrease to negative values after which the negative values gradually increase towards zero. This is because of the initial density of the effective strain, which is positively oriented at zero. We note that in case the effective strain is negatively oriented at zero, the negative values of the displacement velocity increase directly towards positive values after which the values decrease towards zero. This is not shown here. Concerning the effective strain, positive values gradually decrease towards zero and negative values gradually increase towards zero. On day 1, lower bounds of the values approximately are -0.04 and -0.4 for the displacement velocity and effective strain respectively. This reflects the values that are seen in simulations of the full model (not shown here), in which we have seen lower bounds of -0.02 and -0.4. In both plots, the frequencies of the waves do not change.

In case the viscosity is low (Figure 2), all the positive values of the displacement velocity directly decrease towards negative values after which the negative values gradually increase towards zero. At the time when the displacement velocity density becomes zero, the density oscillates around zero with highest amplitude in the middle of the domain of computation. This can be seen in the left plot, where the density is positive on day 1 and negative on day 3. Slowly, the displacement velocity density reaches equilibrium. From the right plot we can see that at the boundaries, the effective strain values deviates from the equilibrium values. Video's show that there is a wave-like pattern that

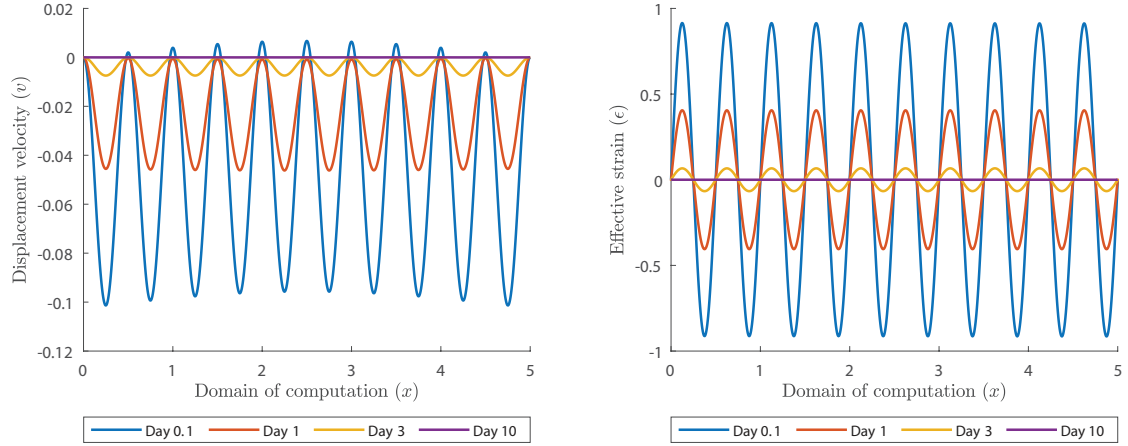


Figure 1: Evolution of mechanics for  $\alpha = 0.22$  and  $\mu = 100$ . The left plot shows the displacement velocity and the right plot shows the effective strain. The initial densities with unit amplitudes are not shown. Videos of these simulations are shown in Online Resources 1 and 2

oscillates around zero and reaches equilibrium in a few days. Both the amplitudes of the displacement velocity and effective strain density stay less than the initial amplitudes, and in the plot of the displacement velocity is it clear that the frequency of the waves changes in time and that convergence is non-monotonic due to non-real eigenvalues.

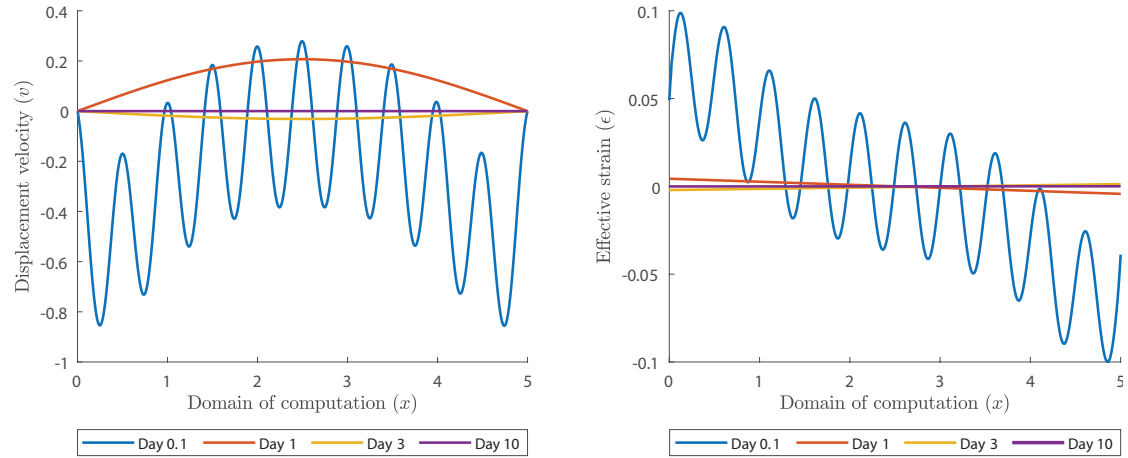


Figure 2: Evolution of mechanics for  $\alpha = 0.22$  and  $\mu = 1$ . The left plot shows the displacement velocity and the right plot shows the effective strain. The initial densities with unit amplitudes are not shown. Videos of these simulations are shown in Online Resources 3 and 4

The main difference between the input values in Figures 1 and 2 is the value of the viscosity. If the viscosity is set to a large value, then from the stability analysis it follows

that the model converges faster and monotonically towards the equilibrium. From a biological perspective, a large value of the viscosity mimics a large amount of damping, and this damping term makes the equation for the displacement velocity more ‘diffusive’. A diffusion equation satisfies a maximum principle, that is, the extremes can only be assumed on the boundary of the domain or initially, unless the solution is constant. This implies that the solution must behave more monotonically for large viscosities.

We are interested in the case where  $\alpha = 0$ . For positive eigenvalues, Theorem 1 requires that  $\mu \geq \frac{\sqrt{\rho_t E \sqrt{\bar{\rho}} (1 - \epsilon_0)}}{\pi} |\Omega|$  in case  $k = 1$ . In case the viscosity is large enough, the simulations show similar behavior as seen in Figure 1. However, the results are different for a low viscosity, as seen in Figure 3. In comparison with the case where  $a > 0$ , the amplitudes of the displacement velocity density become larger in the case where  $\alpha = 0$ . The displacement velocity density still oscillates between positive and negative values, as seen in the left plot of Figure 2, though with larger amplitudes. Furthermore, it takes more time to reach equilibrium. From the right plot we can see that on the boundaries, the effective strain again initially deviates from equilibrium. This reflects the fact that in case  $\alpha = 0$ ,  $\lim_{t \rightarrow \infty} \epsilon(x, t) = \epsilon_0 \in \mathbb{R}$ . The effective strain density oscillates around it’s equilibrium, until it reaches it after about 50 days.

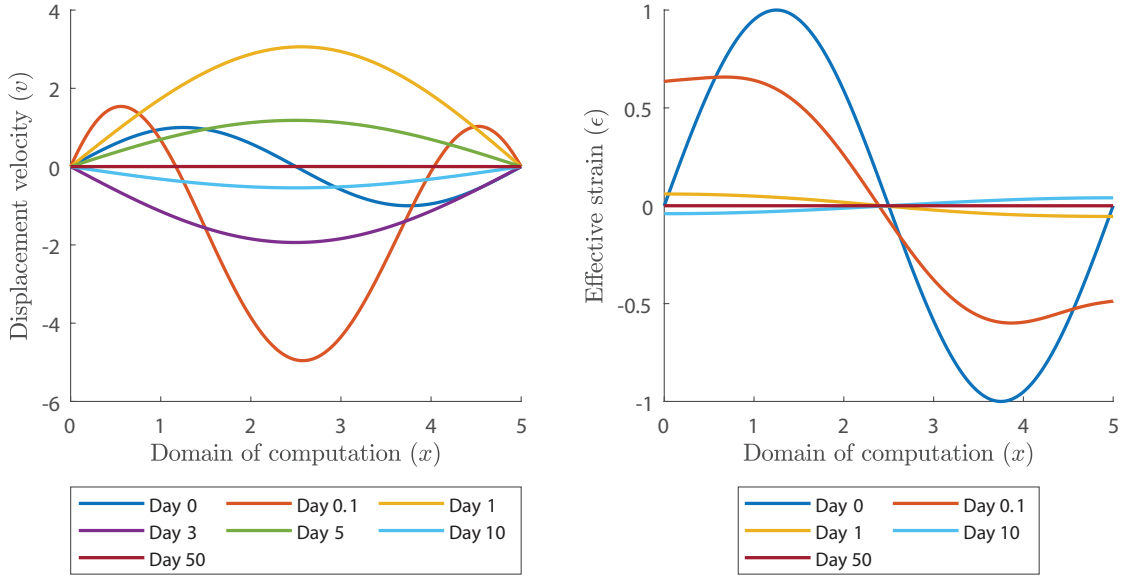


Figure 3: Evolution of mechanics for parameters  $\alpha = 0$  and  $\mu = 1$ . The left plot shows the displacement velocity and the right plot shows the effective strain. Videos of these simulations are shown in Online Resources 5 and 6

Other figures confirm the unconditional stability for the discrete system as well. These figures are not shown here.

## 5.2 Validation of the stability of the one-dimensional transport model

To validate the stability for the reaction-transport equations, we perturb the initial density of the fibroblasts, the myofibroblasts, the chemokines and collagen. We use two levels ( $5 \times 10^{-4}$  and  $3 \times 10^{-4}$ ) for the chemokine decay rate  $\delta_c$ . We use 200 elements to divide the domain of computation between 0 and 1, which represents half a domain of a wound on which we perform computations. This is possible due to the symmetry of the model. We perturb the initial density of the fibroblasts and collagen by using a sine function with amplitude 10 and  $10^{-2}$ , respectively. This is possible because the equilibrium densities of the fibroblasts and collagen are non-zero. For the initial density of the myofibroblasts and chemokines we use uniform splines with 21 knots. On the boundaries, the knots have zero value, and in between the values are 6 and 3 for the myofibroblasts, and  $2 \times 10^{-15}$  and  $0.5 \times 10^{-15}$  for the chemokines. This way we ensure that the myofibroblast and chemokine density values are positive. We show the most significant simulation results.

Figure 4 shows the evolution of the constituents in case the eigenvalues are real-valued. We see that within 400 days, the fibroblasts, the myofibroblasts and the chemokines reach the equilibrium, while collagen take a longer time to reach equilibrium. Because of the initial perturbation, the fibroblasts are reduced at the right boundary, while the myofibroblasts and the chemokines are increased at the right boundary. Hence, the fibroblasts increase after one day, while the myofibroblasts and chemokines decrease after one day. The collagen density shows normal behavior, where all values gradually move towards the equilibrium density  $\bar{\rho} = 0.1125$ .

From a biological perspective, one can say that the model pushes the differences in fibroblasts to the center of the wound, yielding a reduced number of cells at the center of the wound. The number of myofibroblasts is therefore quickly reduced, as well as the appearance of chemokines, since the values of the variables do not balance the model until equilibria are reached. It is highly likely that this change in distributions and density is mostly because of random and directed movement of cells and molecules. Since collagen lacks this kind of movement (i.e., eq. (13)), the density of these fibrils and bundles changes because of the chemical reaction. That is, the secretion of collagen at points in the wound where the density is below equilibrium and the decay of collagen at the points in the wound where the density is above equilibrium.

In order to show the implication from the stability constraint for the chemicals, we perturbed the initial conditions and set the chemokine decay rate  $\delta_c$  such that  $\delta_c < \frac{k_c}{a^{II}\bar{\rho}}$ . We simulated for 1200 days. Figure 5 shows the evolution of the chemokines on the first 16 days and Figure 6 shows the evolution of all the constituents from different days on. In comparison with Figure 4, we see from Figure 5 that the density of the chemokines does not decrease towards the expected zero equilibrium, but increases fastly in case the stability constraint is not met. From a biological perspective, one can say that too much chemokines are secreted in contrast to too less chemokines that decay. This leads to an abundance of chemokines at the center of the wound which has great influence on the evolution of the other constituents from day 16 on. In case the stability constraint is not met, the evolution of the densities of the fibroblasts, the myofibroblasts and collagen



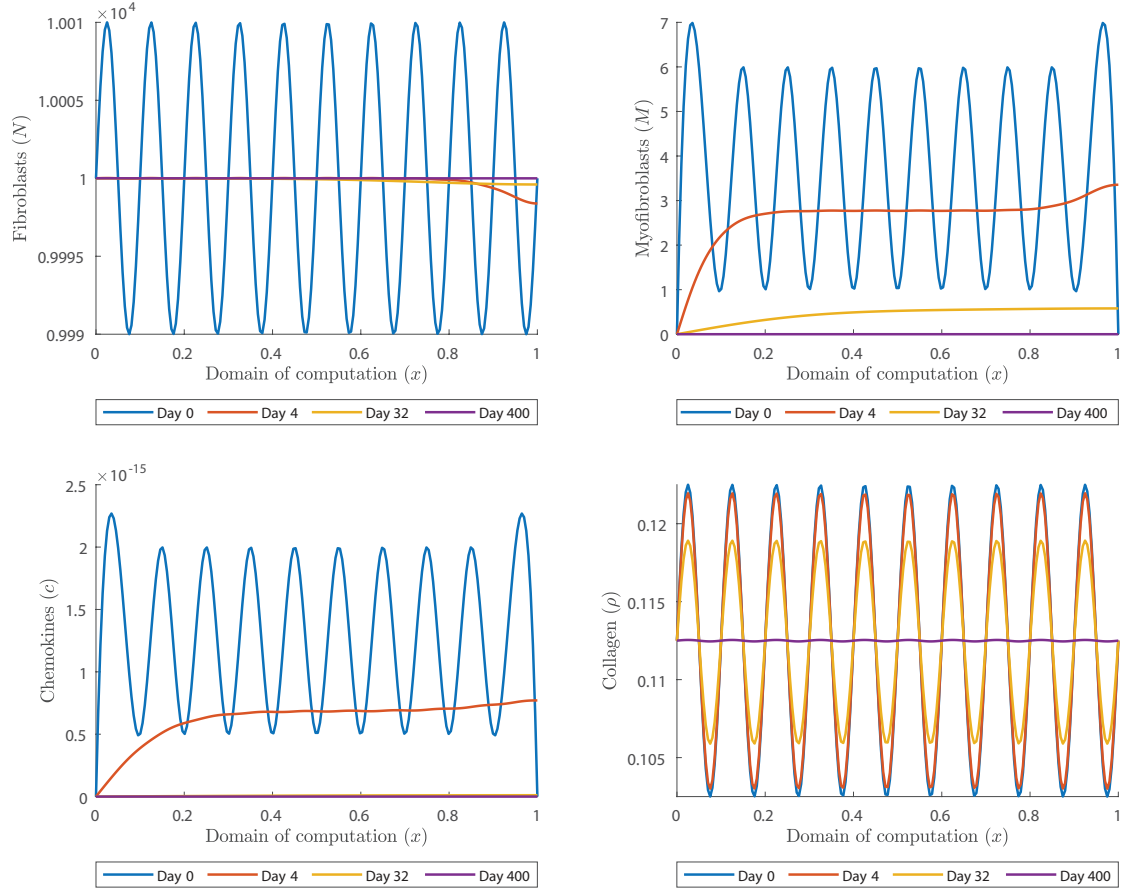


Figure 4: Evolution of the constituents for parameters  $\delta_c = 5 \times 10^{-4}$  and  $k = 10$ . The values for all other parameters are equal to those shown in Table 1, which can be found in the Appendix. Videos of these simulations are shown in Online Resources 7, 8, 9 and 10

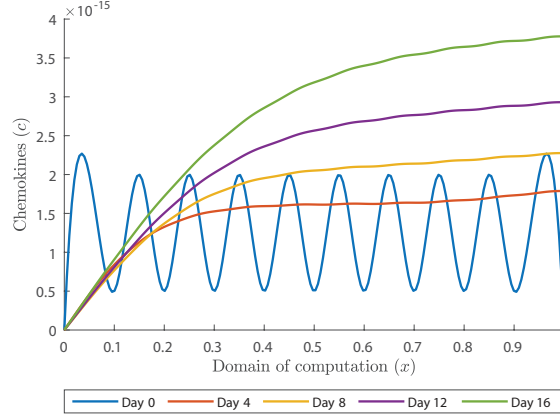


Figure 5: Evolution of the chemokines on the first 16 days for parameter  $\delta_c = 3 \times 10^{-4}$ . The values for all other parameters are equal to those shown in Table 1, which can be found in the Appendix

on the first 16 days are comparable with the evolution of these constituents in case the stability constraint is met.

Figure 6 shows the effect of the increasing amount of chemokines at the center of the wound. From the lower left plot we can see that the chemokine density is very unstable. The positive value at the right boundary increases immediately and does not decrease before 232 days. After that, the chemokine density starts moving towards the expected zero equilibrium, but moves away again from day 344, until it reaches a new equilibrium around day 1200. In fact, the chemokine density oscillates around this new equilibrium. The increase of the chemokine density at the center of the wound has an effect on the fibroblast and myofibroblast cell distribution, which can be seen in the upper left and right plots of Figure 6. The fibroblast cell distribution initially moves towards its expected equilibrium (not shown here). However, after 38 days the right boundary of the distribution quickly moves away from this equilibrium until it reaches maximum deviation from the expected equilibrium on day 268. After that, the fibroblast cell distribution oscillates around its new equilibrium that deviates about 275 cells/cm<sup>3</sup> from 10<sup>4</sup> cells/cm<sup>3</sup> at the center of the wound. The same oscillating effect can be seen in the upper right plot. The myofibroblast cell distribution initially moves towards zero, but increases rapidly after 38 days (not shown here) until it reaches maximum deviation from the expected equilibrium on day 240. After that, the myofibroblast cell distribution oscillates around its new equilibrium that deviates about 75 cells/cm<sup>3</sup> from zero at the center of the wound. The collagen density evolves a bit different. Like the other constituents, the collagen density oscillates around its new equilibrium that deviates from the expected equilibrium by 0.0222 g/cm<sup>3</sup>. However, the initial waves of the perturbation are still visible on day 260 in the lower right plot, while these initial waves already vanished in the other plots. Other figures, which are not shown here, show that fast oscillating perturbations vanish. This can be seen by setting  $k$  or  $\beta$  to very high

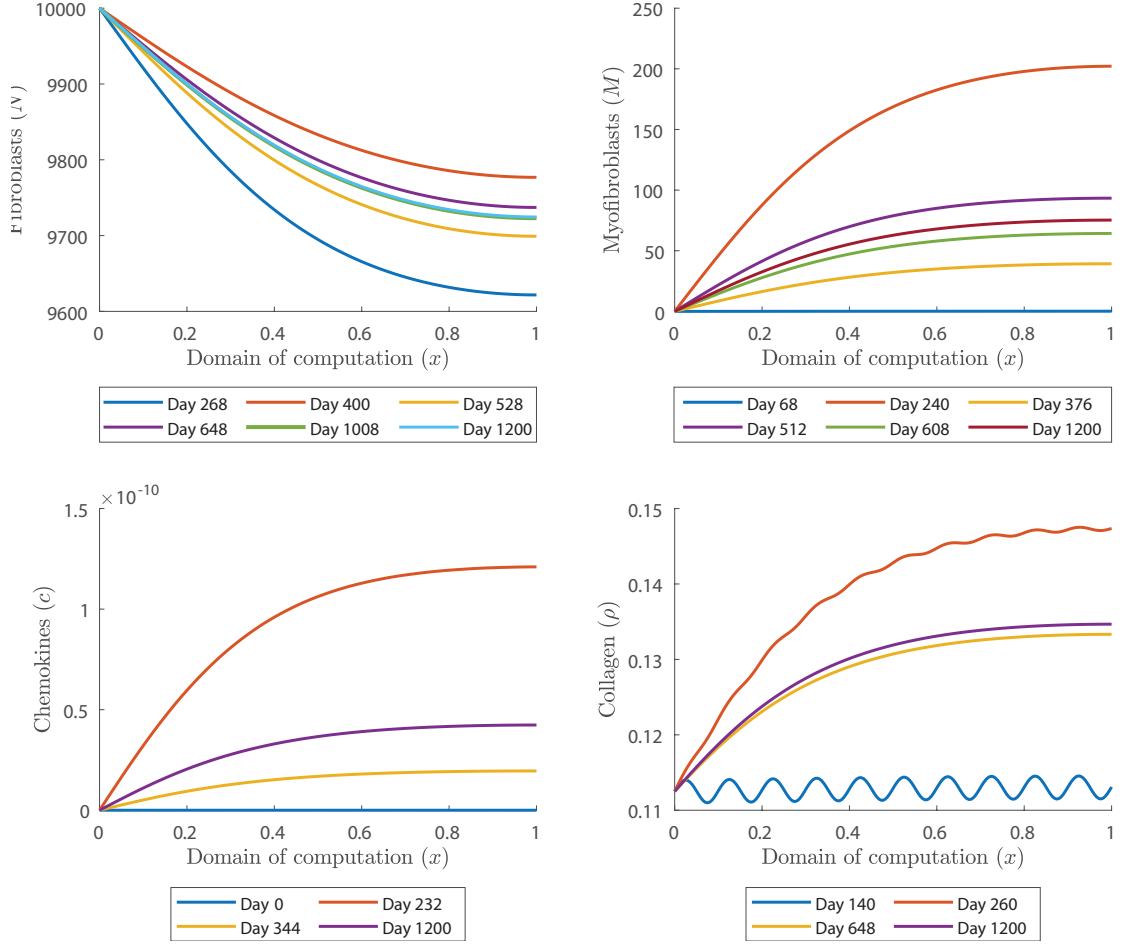


Figure 6: Evolution of the constituents for parameters  $\delta_c = 3 \times 10^{-4}$  and  $k = 1$ . The values for all other parameters are equal to those shown in Table 1, which can be found in the Appendix. Videos of these oscillations are shown in Online Resources 11, 12, 13 and 14

values in equations (56) and (69), respectively. However, fast oscillating perturbations do not change the overall behavior that we have seen in Figure 6.

## 6 Discussion

In this study, we investigate the stability of the one-dimensional model for intensity of contraction and the formation of contractures in burn scars. The model presented in this paper is the one-dimensional version of the morphoelastic model developed by Koppenol. This model is based on the theory and derivations developed by Hall (2008). We incorporated four constituents: fibroblasts, myofibroblasts, chemokines, and collagen. Furthermore, we use equations for the displacement of the dermal layer, the displacement velocity of the dermal layer, and the effective Eulerian strain present in the dermal layer.

We presented a stability analysis for the mechanical model  $(v, \epsilon)$  as well as for the chemical model  $(N, M, c, \rho)$ . For the mechanical model we distinguished between two cases: the model without plastic deformation (elasticity) and the model with plastic deformation (morphoelasticity). For the elastic model (i.e.,  $\alpha = 0$ ), we have shown that the equilibrium distribution of the effective strain should be less than 1 ( $\bar{\epsilon} \leq 1$ ), and that the parameter that represents the viscosity of skin should be greater or equal to a factor containing the total mass density of dermal tissues, the Young's Modulus and the equilibrium distribution of the effective strain. We have shown that there exists a consistency between the eigenvalues of the discrete model, which is used for the uniform grid based finite element approximation, and the eigenvalues of the continuous model, which is the 'true' model. The difference in the eigenvalues between these two models is of order  $\mathcal{O}(h^2)$ . With simulations we have shown that the stability criterion needs to be met in order to prevent the model to increase the amplitudes of the initial perturbations, in case of the elastic model. However, this does not induce instability in terms of equilibria. All the simulations have shown that the modeled displacement velocity and effective strain eventually reach their equilibrium densities.

For morphoelasticity (i.e.,  $\alpha > 0$ ), we have shown that stability is guaranteed for any perturbation of the equilibrium densities. In case the viscosity is low, the figures show that the displacement velocity as well as the effective strain reach their equilibrium densities. Though, in this case convergence is not monotonic, but oscillates as seen in Figure 2.

We also provided a stability analysis for the chemical model. A surprising result was that we could derive the eigenvalues of the matrix involved in the stability of the chemical equations analytically. This is possible because the linearization of equation (43) leaves out other variables after accounting for the equilibria values. As a result, we could say that three of the four eigenvalues meet the stability constraints independent of the chosen value for the parameters, given that the parameters involved are positive. Therefore, only one stability constraint is needed to assure stable results after perturbations. This stability constraint states that the model is stable on the condition that the decay rate of the chemokines is greater than a factor concerning the maximum net secretion rate

of the chemokines, the concentration of the chemokines that causes half-maximum net secretion rate of the chemokines, and the collagen equilibrium density. We have shown that also in the chemical model there exists a consistency between the discrete model and the continuous model. The differences between the eigenvalues of these models are again of order  $\mathcal{O}(h^2)$ . With simulations we validated the stability constraint. If initial distributions and densities are perturbed, then it takes some time to bring the distributions and densities back to equilibrium values. In case the stability constraint is met, then the fibroblasts, the myofibroblasts, the chemokines and collagen gradually move towards their equilibria. If the stability constraint is not met, then the chemokines move away from equilibrium and thereby effect the distributions of the fibroblasts and the myofibroblasts, yielding unrealistic plots. All the constituents move away from the expected equilibria and oscillate around new equilibria. The collagen density still shows the initial waves of the perturbations around day 260, while these waves already vanished in the other densities. Taken together, the numerical model fully reproduces the stability constraints.

It would be interesting to incorporate hypertrophy to this one-dimensional morphoelastic model Koppenol et al. (2017), since hypertrophic scars can also develop contractions. The beauty of the one-dimensional model is the speed, hence incorporation of hypertrophy will quickly yields new results and therefore insight. Another interesting direction is to model the boundaries of the wounded area as elastic springs, since with the current setting the boundary of the domain of computation needs to be “sufficiently far away”. Furthermore, we are working on a sensitivity analysis and feasibility study for the one-dimensional morphoelastic model. It would be interesting to combine the hypertrophic one-dimensional model with the one-dimensional morphoelastic model and perform these analyses on the combined model as well. One other interesting approach is to extend the equations to account for growth of children. A first attempt will be to add another factor in equation (21).

## Acknowledgements

The authors are grateful for the financial support by the Dutch Burns Foundation under Project 17.105.

## Conflict of interest

The authors declare that they have no conflict of interest.

## Appendix

In the appendix one finds the stiffness matrices, element vectors of the chemical model, and the parameter values.

For the chemokines we have the following stiffness matrix:

$$\mathcal{S}_{ij}^c \simeq \frac{D_c}{|e_p|} \begin{bmatrix} 1 & -1 \\ -1 & 1 \end{bmatrix} - \frac{|e_p|}{2} \begin{bmatrix} f^c(x_p, t) & 0 \\ 0 & f^c(x_{p+1}, t) \end{bmatrix}, \quad (83)$$

where

$$f^c(x, t) = \left[ \frac{k_c}{a_c^{II} + c} \right] [N + \eta^I M] - \delta_c \frac{[N + \eta^{II} M] \rho}{1 + a_c^{III} c}. \quad (84)$$

For the fibroblasts we have the following stiffness matrix:

$$\begin{aligned} \mathcal{S}_{ij}^N \simeq & \frac{D_F}{2|e_p|} (N(x_p, t) + M(x_p, t) + N(x_{p+1}, t) + M(x_{p+1}, t)) \begin{bmatrix} 1 & -1 \\ -1 & 1 \end{bmatrix} \\ & - \frac{\chi_F}{2} \begin{bmatrix} -\frac{dc(x_p, t)}{dx} & -\frac{dc(x_{p+1}, t)}{dx} \\ \frac{dc(x_p, t)}{dx} & \frac{dc(x_{p+1}, t)}{dx} \end{bmatrix} \\ & - \frac{|e_p|}{2} \begin{bmatrix} f^N(x_p, t) - k_F c(x_p, t) & 0 \\ 0 & f^N(x_{p+1}, t) - k_F c(x_{p+1}, t) \end{bmatrix} + \frac{|e_p|}{6} \delta_N \begin{bmatrix} 2 & 1 \\ 1 & 2 \end{bmatrix}, \end{aligned} \quad (85)$$

where

$$f^N(x, t) = r_F \left[ 1 + \frac{r_F^{\max} c}{a_c^I + c} \right] [1 - \kappa_F(N + M)] N^q. \quad (86)$$

For the myofibroblasts we have the following stiffness matrix:

$$\begin{aligned} \mathcal{S}_{ij}^M \simeq & \frac{D_F}{2|e_p|} (M(x_p, t) + N(x_p, t) + M(x_{p+1}, t) + N(x_{p+1}, t)) \begin{bmatrix} 1 & -1 \\ -1 & 1 \end{bmatrix} \\ & - \frac{\chi_F}{2} \begin{bmatrix} -\frac{dc(x_p, t)}{dx} & -\frac{dc(x_{p+1}, t)}{dx} \\ \frac{dc(x_p, t)}{dx} & \frac{dc(x_{p+1}, t)}{dx} \end{bmatrix} - \frac{|e_p|}{2} \begin{bmatrix} f^M(x_p, t) & 0 \\ 0 & f^M(x_{p+1}, t) \end{bmatrix} + \frac{|e_p|}{6} \delta_M \begin{bmatrix} 2 & 1 \\ 1 & 2 \end{bmatrix}, \end{aligned} \quad (87)$$

where

$$f(x, t)^M = r_F \left\{ \frac{[1 + r_F^{\max} c]}{a_c^I + c} \right\} [1 - \kappa_F(N + M)] M^q. \quad (88)$$

We have the following element vector:

$$\mathcal{F}_i^M \simeq \frac{|e_p|}{2} k_F \begin{bmatrix} c(x_p, t) N(x_p, t) \\ c(x_{p+1}, t) N(x_{p+1}, t) \end{bmatrix}. \quad (89)$$

For collagen we have the following stiffness matrix:

$$\mathcal{S}_{ij}^\rho \simeq \frac{|e_p|}{2} \begin{bmatrix} g^\rho(x_p, t) & 0 \\ 0 & g^\rho(x_{p+1}, t) \end{bmatrix}, \quad (90)$$

where

$$g^\rho(x, t) = \delta_\rho \frac{[N + \eta^{II} M] \rho}{1 + a_c^{III} c}. \quad (91)$$

We have the following element vector:

$$\mathcal{F}_i^\rho \simeq \frac{|e_p|}{2} \begin{bmatrix} f^\rho(x_p, t) \\ f^\rho(x_{p+1}, t) \end{bmatrix}, \quad (92)$$

where

$$f(x, t)^\rho = k_\rho \left\{ 1 + \left[ \frac{k_\rho^{\max} c}{a_c^{IV} + c} \right] \right\} [N + \eta^I M]. \quad (93)$$

## References

- Barocas, V. H. and Tranquillo, R. (1997). An anisotropic biphasic theory of tissue-equivalent mechanics: The interplay among cell traction, fibrillar network deformation, fibril alignment, and cell contact guidance. *Journal of Biomechanical Engineering*, 119(2):137–145.
- Dallon, J., Sherrat, J., and Maini, P. (1999). Mathematical modelling of extracellular matrix dynamics using discrete cells: Fiber orientation and tissue regeneration. *Journal of Theoretical Biology*, 199(4):449–471.
- Enoch, S. and Leaper, D. (2008). Basic science of wound healing. *Surgery (Oxford)*, 26(2):31–37.
- Garrison, G., Huang, S. K., Okunishi, K., Scott, J. P., Penke, L. R. K., Scruggs, A. M., and Peters-Golden, M. (2013). Reversal of myofibroblast differentiation by prostaglandin e2. *American Journal of Respiratory Cell and Molecular Biology*, 48(5):550–558.
- Hall, C. L. (2008). *Modelling of some biological materials using continuum mechanics*. PhD thesis, Queensland University of Technology.
- Koppenol, D. (2017). *Biomedical implications from mathematical models for the simulation of dermal wound healing*. PhD thesis, Delft University of Technology.
- Koppenol, D., Vermolen, F., and Niessen, F. e. a. (2017). A mathematical model for the simulation of the formation and the subsequent regression of hypertrophic scar tissue after dermal wounding. *Biomech Model Mechanobiol*, 16(1):15–32.
- McDougall, S., Dallon, J., Sherrat, J., and Maini, P. (2006). Fibroblast migration and collagen deposition during dermal wound healing: Mathematical modelling and clinical implications. *Philosophical Transactions of the Royal Society A: Mathematical, Physical and Engineering Sciences*, 364(1843):1385–1405.
- Menon, S. N., Hall, C. L., McCue, S. W., and McElwain, D. L. S. (2017). A model for one-dimensional morphoelasticity and its application to fibroblast-populated collagen lattices. *Biomechanics and Modeling in Mechanobiology*, 16(5):1743–1763.

Table 1: Overview of the parameters used for the simulations. Shown are the descriptions, values and dimensions.

Description	Symbol	Value	Dimension
Chemokine diffusion coefficient	$D_c$	$2.88 \times 10^{-3}$	$\text{cm}^2/\text{day}$
Cell diffusion coefficient	$D_F$	$10^{-7}$	$\text{cm}^5/(\text{cells day})$
Cell chemotaxis coefficient	$\chi_F$	$3 \times 10^{-7}$	$\text{cm}^5/(\text{g day})$
Chemokine max. net secretion rate	$k_c$	$4 \times 10^{-13}$	$\text{g}/(\text{cells day})$
Cell division rate	$r_F$	$9.24 \times 10^{-1}$	$\text{cm}^{3q}/(\text{cells}^q \text{ day})$
Division rate max. enhancer	$r_F^{\max}$	2	-
Secretion rate max. enhancer	$k_p^{\max}$	10	-
Division rate half-max. enhancer	$a_c^I$	$10^{-8}$	$\text{g}/\text{cm}^3$
Secretion rate half-max. enhancer	$a_c^{II}$	$10^{-8}$	$\text{g}/\text{cm}^3$
MMP secretion inhibitor	$a_c^{III}$	$2 \times 10^8$	$\text{cm}^3/\text{g}$
Secretion rate half-max. enhancer	$a_c^{IV}$	$10^{-9}$	$\text{g}/\text{cm}^3$
Ratio of myofibroblasts to fibroblasts in secretion of chemokines	$\eta^I$	2	-
Ratio of myofibroblasts to fibroblasts in secretion of MMPs	$\eta^{II}$	$5 \times 10^{-1}$	-
Cell differentiation rate	$k_F$	$1.08 \times 10^{-7}$	$\text{cm}^3/(\text{g day})$
Cell division rate reduction factor	$\kappa_F$	$10^{-6}$	$\text{cm}^3/\text{cells}$
Fibroblast apoptosis rate	$\delta_N$	$2 \times 10^{-2}$	$/\text{day}$
Myofibroblast apoptosis rate	$\delta_M$	$6 \times 10^{-2}$	$/\text{day}$
Collagen decay rate	$\delta_\rho$	$6 \times 10^{-6}$	$\text{cm}^6/(\text{cells g day})$
Fibroblast equilibrium distribution	$\bar{N}$	$10^4$	$\text{cells}/\text{cm}^3$
Myofibroblast equilibrium distribution	$\bar{M}$	0	$\text{cells}/\text{cm}^3$
Chemokine equilibrium density	$\bar{c}$	0	$\text{g}/\text{cm}^3$
Collagen equilibrium density	$\bar{\rho}$	$1.125 \times 10^{-1}$	$\text{g}/\text{cm}^3$
Total mass density of dermal tissues	$\rho_t$	1.09	$\text{g}/\text{cm}^3$
Constant in Young's Modulus	$E$	$2.1 \times 10^2$	$\text{N}/((\text{g cm})^{0.5})$



- Olsen, L., Sherratt, J., and Maini, P. (1995). A mechanochemical model for adult dermal wound contraction and the permanence of the contracted tissue displacement profile. *Journal of Theoretical Biology*, 177(2):113–128.
- Ramtani, S. (2004). Mechanical modelling of cell/ecm and cell/cell interactions during the contraction of a fibroblast-populated collagen microsphere: theory and model simulation. *Journal of Biomechanics*, 37(11):1709–1718.
- Ramtani, S. and et al (2002). Remodeled-matrix contraction by fibroblasts: numerical investigations. *Computers in Biology and Medicine*, 32(4):283–296.
- Tranquillo, R. and Murray, J. D. (1992). Continuum model of fibroblast-driven wound contraction: Inflammation-mediation. *Journal of Theoretical Biology*, 158(2):135–172.
- Van Kan, J., Segal, A., and Vermolen, F. (2014). *Numerical Methods in Scientific Computing*. Delft Academic Press, 2nd edition.
- Wang, Y. e. (2018). Burn injury: Challenges and advances in burn wound healing, infection, pain and scarring. *Advanced Drug Delivery Reviews*, 123:3–17.
- WHO (2018). World health organisation, fact sheet, burns, 06-03-2018. <https://www.who.int/en/news-room/fact-sheets/detail/burns>. Accessed on 04-12-2019.
- Young, A. and McNaught, C. (2011). The physiology of wound healing. *Surgery (Oxford)*, 29(10):475–479.